

# Journal of Mechanics of Materials and Structures

**COMBINED EFFECTS OF INTERSTITIAL AND LAPLACE PRESSURE  
IN HOT ISOSTATIC PRESSING OF CYLINDRICAL SPECIMENS**

Laura Galuppi and Luca Deseri

**Volume 9, No. 1**

**January 2014**





## COMBINED EFFECTS OF INTERSTITIAL AND LAPLACE PRESSURE IN HOT ISOSTATIC PRESSING OF CYLINDRICAL SPECIMENS

LAURA GALUPPI AND LUCA DESERI

Sintering of precompacted metallic and ceramic micro and nanopowders is a complex problem influenced by several factors. We quantify the influence of both local capillary stresses acting at the surface of one pore or particle (usually referred to as Laplace pressure) and the gas pressure in pores during sintering of precompacted metallic (micro/nano)powdered cylinders. The latter influences only the third phase of sintering, that is, the phase in which the porosity is closed.

The isostatic pressing loading mode, which also covers the case of free sintering, is considered. Whereas the Laplace pressure is demonstrated to have a beneficial effect on sintering, the gas pressure acts against the reduction of the porosity, causing an increase in sintering time. This contribution could reach the sum of the stress due to loading and the interstitial pressure, thereby preventing the desired porosity to be reached.

For the sake of illustration, a specific aluminum-zinc-magnesium-copper alloy is examined in this paper. The purpose is to estimate the effects of sintering time and residual porosity and to determine thresholds under which the contributions described above are negligible. In order to determine the effects of Laplace and gas pressure in pores on the stability of the process, a high-order perturbation analysis has been performed.

### 1. Introduction

In recent decades, powder technology has become one of the most important technological processes for the production of metallic and ceramics components. Free sintering, hot isostatic pressing (HIP), and hot forging are different ways to realize a key phase in which the primary mechanical properties of the final material are obtained. In order to be able to predict the final structure of a body undergoing such a process, it is crucial to define an analytical theory of sintering allowing one to follow the evolution of the mechanical properties of the material (determined by this structure) during sintering, and to get the final features of the compound at the end of this process.

The foundations of the analytical study of sintering processes were laid down in the 70s (see, for example, [Skorohod 1972; Ashby 1974; Coleman and Beere 1975]) and many studies gave important new results in the 90s [Duva and Crow 1992; Cocks 1994; Olevsky and Molinari 2000]. In recent years, several papers have improved knowledge of sintering processes. This has been done both from analytical (see, among others, [Olevsky et al. 2006; Maximenko et al. 2012; Wakai 2013]) and experimental (see, for example, [Guillon et al. 2008; Sankar et al. 2011]) points of view; the latter is usually focused on new materials and techniques. An innovative sintering technique, widely developed and used in recent years,

---

*Keywords:* sintering, powder technology, nanopowders, hot isostatic pressing, interstitial and Laplace pressure, ceramic compaction, metallic powder compaction .

is spark plasma sintering (SPS), in which materials are compacted and condensed to higher densities. Systems designed for SPS use direct current pulses to create spark energy between the particles of the material. This technology achieves rapid fusing between particles and, unlike other sintering processes that are solely involved in metalworking, SPS can be applied to ceramics, composite materials, and nanostructures. The compaction of samples can be achieved in a relatively short time period, making SPS a very promising technique for elaborate nanostructured materials. Several studies have recently been performed on this technique [Munir et al. 2006; Schwarz et al. 2012; Wolff et al. 2012].

The present work is focused on modeling the evolution of material properties during sintering of axisymmetric samples. It is a natural extension of [Olevsky and Molinari 2006], dealing with an analysis of the kinetics and stability of porous axially symmetric bodies undergoing sintering under different loading modes. In that paper, in addition to an extensive review of the available literature, both about modeling of sintered materials obtained by compacted powders (see, for example, [Bigoni and Piccolroaz 2004; Piccolroaz et al. 2006a; 2006b]) and constitutive equations for porous media, the problem is solved for the cases in which both the interstitial stress (due to the pressure exerted by the gas in the pores) and the Laplace pressure (due to the surface tension at the interfaces between matrix and pores) are negligible compared with the external loading. The strategy introduced in [Olevsky and Molinari 2006] appears to be the most effective among the possibilities for predicting the kinetics of bodies undergoing sintering (even for the simple geometry mentioned above). More modern formulations dealing with multiscale mechanics may also be conceived to deliver more accurate micromechanics-based approaches to sintering (see, for example, [Deseri and Owen 2003; 2010; 2013; Paola and Zingales 2011; 2012; Dal Corso and Deseri 2013; Deseri et al. 2013; Paola et al. 2013], among many others).

Even though sintering is an inhomogeneous process, not only due to the inhomogeneity of the properties of the powder particles but also to internal stresses that can arise either from external constraints, differential densification [Green et al. 2008], or particle rearrangement during sintering [Wakai et al. 2007; Lee et al. 2012], in this work only the average state of the stress is considered. This is motivated by the observation, pointed out in [Olevsky and Molinari 2006], that the assumption of homogeneous plane stress through a sample is reasonable even in the case of a nonuniform cross-section (see, for example, [Hutchinson et al. 1978] for tensile tests). Incidentally, this is equivalent to assuming that specimens undergo constant states of (plane) stresses corresponding to the average of the actual stress fields. The approach suggested by the assumptions above has the advantage of capturing the essentials of both kinetics and stability, avoiding searching for the solutions of complicated (initial) boundary value problems. Nevertheless, in [Olevsky and Molinari 2006], this strategy has been employed only for cases in which the effect of the Laplace pressure is negligible with respect to the applied stresses. Hence it needs to be extended to the case of moderate stresses in comparison with the interstitial gas pressure.

Here we consider ideal processes where stresses are kept constant, unlike in [Olevsky and Molinari 2006], where, instead, a fictitious external load replaces the role of the stress.

This paper is outlined as follows. In Section 2, the theory of sintering introduced in [Olevsky 1998; Olevsky and Molinari 2006] is essentially summarized and specialized for the case of isostatic pressing processes, emphasizing the role of the Laplace pressure and the gas pressure in pores. In Section 2.3, the two most-used ways to get the relationship between the porosity (defined as the ratio of the volume of pores and the total volume of the sintered material) and the Laplace pressure (also called the *sintering*

*stress*) are revisited; furthermore, the model for obtaining such a pressure based on the microscopic dissipation is shown to be compatible with the incompressibility of the matrix if and only if the material is nonlinearly viscous. Analogously, in Section 2.4 a practical way to account for the interstitial stress (that is, the gas pressure in pores) is proposed.

In Section 3, the effect of the Laplace pressure on the evolution of the porosity in sintering processes entailing isostatic pressing is studied. An accurate comparison among different models of the normalized shear and bulk moduli of the material and between the two different expressions for the sintering is performed. In Section 3.1, two issues are investigated. First of all, thresholds on stresses caused by external loads are determined, under which the influence of the interstitial pressure cannot be neglected. Such thresholds may be strongly influenced by the strain rate sensitivity of the material and the average radius of the particles; this feature may have a stronger impact for nanostructured powders. Furthermore, the discrepancy between the values of the residual porosity is evaluated by neglecting or accounting for the Laplace pressure in sintering processes of a given time-duration. In Section 4, an analogous analysis is performed regarding the effect of gas pressure in pores in isostatic pressing sintering processes. In performing such analysis, two cases may arise through a comparison between the stress caused by external loading and Laplace pressure (sintering driving) and gas pressure in pores (opposing the reduction of the porosity). In particular, the occurrence of equality between such values can be reached at a definite (critical) porosity, which remains constant at a limit value. It is clear that, if this value is greater than the desired porosity at the end of the process, this cannot be obtained.

Finally, in Section 5, the stability of the process, namely of the solution of the problem in terms of the time evolution of the porosity obtained in Section 2, is performed in two steps along the lines traced in [Olevsky and Molinari 2006]. A lower-order analysis is performed in Section 5.1, where perturbations on the porosity alone are considered. In Sections 5.2 and 5.3, a higher-order analysis is performed by perturbing, together with the porosity, the reference value of the Laplace pressure and the gas pressure in pores; this more refined analysis shows that the effect of the latter is to reduce the stability of the process. The Appendix is devoted to analyzing free sintering processes. In particular, since no external stress is applied, it is crucial to examine to what extent different ways of evaluating the Laplace pressure may influence the outcome in terms of the evolution of the porosity. Hence, a parametric analysis in terms of the given temperature is performed to estimate the sintering time for a prescribed target residual porosity.

## 2. Theory of sintering and kinetics of porosity

The sintering process is classically divided into three phases [Swinkels and Ashby 1981; Swinkels et al. 1983; Cocks 1994]:

- A first stage in which the particles are brought into contact and necks grow at the particle contacts; in this phase, the material may be modeled as an aggregate of individual particles with little contact. For crystalline materials, this phase involves diffusion of vacancies in the crystal lattice, whereas noncrystalline materials sinter by viscous flow [Scherer 2001].
- An intermediate second stage in which the material can be idealized as a porous material with connected porosity.
- A third and final phase in which, usually for relative density (that is, as will be discussed in the sequel, the ratio between the volume of the matrix and the total volume of the sintered material)

greater than 90% [Coleman and Beere 1975], i.e., for porosity less than 10%, in which the pores are isolated and spherical. In the sequel, this value of the porosity will be denoted by  $\theta_c$ , called the closure porosity.

It is important to note that in the second phase the pores can be considered quasispherical [Ashby 1974].

The mechanical response of a porous body with nonlinear-viscous behavior (stages 2 and 3) is strongly influenced by the presence of pores (see, for example, [Wakai 2013]) and is described by a rheological constitutive relation, namely:

$$\sigma_{ij} = \frac{\sigma(w)}{w} [\varphi \dot{\varepsilon}'_{ij} + \psi \dot{\varepsilon} \delta_{ij}] + p_L \delta_{ij} - p_I \delta_{ij}, \quad (1)$$

interrelating the components of the stress  $\sigma_{ij}$  and the strain rate  $\dot{\varepsilon}_{ij}$  [Olevsky 1998]. The quantity  $p_L$  represents the Laplace pressure, while the term  $p_I$  represents the gas pressure in the pores. Obviously,  $p_I = 0$  during the first and second phases, since the porosity is open. Here,  $\dot{\varepsilon}'_{ij}$  denotes the  $ij$ -th component of the deviatoric strain rate tensor;  $w$  is the effective equivalent strain rate, defined as

$$w = \frac{1}{\sqrt{1-\theta}} \sqrt{\varphi \dot{\gamma}^2 + \psi \dot{\varepsilon}^2}, \quad (2)$$

where

$$\dot{\varepsilon} = \dot{\varepsilon}_{ii} \quad (3)$$

measures the local shrinking rate (whenever the sintering process entails a volume reduction), and

$$\dot{\gamma} = \sqrt{\dot{\varepsilon}'_{ij} \dot{\varepsilon}'_{ij}} \quad (4)$$

measures the local rate of change in shape. Here and subsequently, index notation with Einstein summation convention is adopted.

The quantity  $p_L$  represents the interstitial pressure produced by the gas contained in the pores; in the sequel we will refer to  $p_L$  as either the ‘‘Laplace pressure’’ or the ‘‘sintering stress’’ (see [Olevsky 1998; Olevsky and Molinari 2000; 2006]).

For further developments, it is convenient to introduce the stress quantities  $p$  and  $\tau$  directly related to shrinking and change in shape, respectively:

$$p = \frac{1}{3} \text{tr} \sigma = \frac{\sigma(w)}{w} \psi \dot{\varepsilon} + p_L - p_I, \quad (5)$$

$$\tau = \sqrt{\sigma'_{ij} \sigma'_{ij}} = \frac{\sigma(w)}{w} \varphi \dot{\gamma}, \quad (6)$$

where  $\sigma'_{ij}$  denotes the  $ij$ -th component of of the deviatoric stress tensor. The quantities  $\varphi$ ,  $\psi$ ,  $p_L$ , and  $p_I$  and their dependence upon the porosity will be treated in Sections 2.2, 2.3, and 2.4.

Let us consider a cylindrical axisymmetric specimen, subject to an external load. The porosity  $\theta$ , defined as the ratio between the pore volume and the total volume [Olevsky and Molinari 2006], is supposed to be constant throughout the sample. This is equivalent to considering the spatial average of the porosity.

From now on, we shall consider average stress distributions of the following form:

$$[\sigma_{ij}] = \begin{bmatrix} \sigma_r & 0 & 0 \\ 0 & \sigma_r & 0 \\ 0 & 0 & \sigma_z \end{bmatrix}, \quad (7)$$

where  $z$  denotes the direction of the axis of the sample and  $r$  is any radial direction. Furthermore, in the sequel, the corresponding average strain rate tensor will be considered. Here,  $\dot{\epsilon}_z$  and  $\dot{\epsilon}_r$  denote the axial and radial strain rates, respectively. Hence,  $\dot{\epsilon}$  and  $\dot{\gamma}$  turn out to be

$$\dot{\epsilon} = \dot{\epsilon}_z + 2\dot{\epsilon}_r, \quad \dot{\gamma} = \sqrt{\frac{2}{3}}|\dot{\epsilon}_z - \dot{\epsilon}_r|. \quad (8)$$

Following [Olevsky and Molinari 2006], one can introduce a loading mode parameter  $n^*$  defined by

$$n^* = \frac{\tau}{p} = \frac{(\sigma(w)/w)\dot{\gamma}}{(\sigma(w)/w)\dot{\epsilon} + p_L - p_I} \quad (9)$$

Similar to the loading mode parameter, it is useful to define a *strain rate mode parameter*  $n$  as

$$n = \frac{\varphi\dot{\gamma}}{\psi\dot{\epsilon}}. \quad (10)$$

The parameter  $n$  assumes the following values for the corresponding loading modes:

- (1)  $n = 0$  for isostatic pressing,
- (2)  $n \rightarrow \infty$  for pure shear ( $p = 0$ ),
- (3)  $n = -\sqrt{6}$  for “free” forging,
- (4)  $n = \sqrt{6}$  for drawing, and
- (5)  $n = \sqrt{\frac{2}{3}} \operatorname{sgn}(\dot{\epsilon}_z)\varphi/\psi$  for constrained forging.

In the sequel, we will consider cases 1, 3, and 5 only.

We refer to “free” forging as the loading mode represented in Figure 1a, a transverse compressive force acting at the top and bottom faces of the sample with no lateral confinement. Hence, the case of constrained forging, shown in Figure 1b, is nothing but an axial compression of the sample in a rigid die.

From (1), (8), and (10), the following relation can be obtained:

$$\sigma_z = \frac{\sigma(w)}{w}\psi\dot{\epsilon}\left[1 + \sqrt{\frac{2}{3}}n \operatorname{sgn}(\dot{\epsilon}_z - \dot{\epsilon}_r)\right] + p_L - p_I; \quad (11)$$

the dependence of the effective equivalent stress  $\sigma(w)$  on the effective equivalent strain rate  $w$  determines the constitutive behavior of a porous material.

Following [Ashby 1990], a power-law mechanism for the deformation is assumed:

$$\frac{\sigma(w)}{\sigma_0} = A\left(\frac{w}{\dot{\epsilon}_0}\right)^m, \quad (12)$$

where  $A$  and  $m$  are material constants ( $A$  is temperature dependent,  $0 < m < 1$ ), and  $\sigma_0$  and  $\dot{\epsilon}_0$  are the reference stress and reference strain rate, respectively. The two limiting cases corresponding to ideal plasticity and linear viscosity are given by  $m = 0$  and  $m = 1$ , respectively.

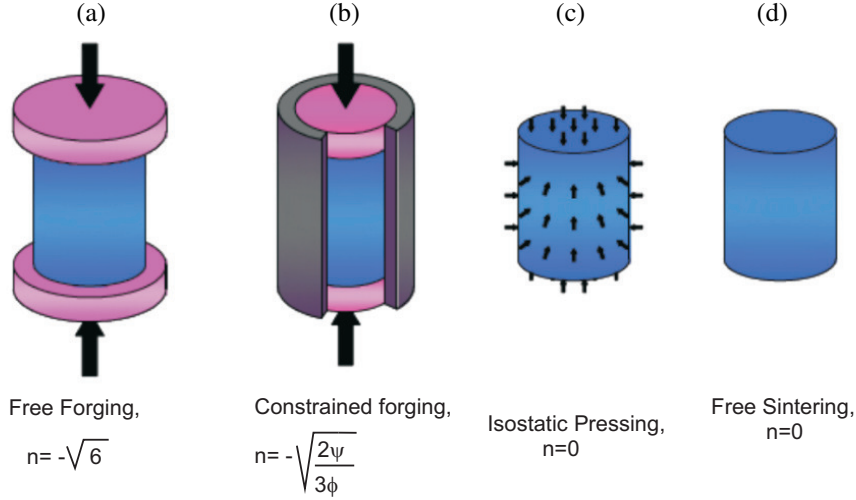


**Figure 1.** Different loading modes.

Equations (12) and (2) can be used to obtain an explicit expression for the ratio between the effective equivalent stress  $\sigma(w)$  and the effective equivalent strain rate  $w$  in terms of the porosity, the normalized shear and bulk moduli, the loading mode, and the shrinking rate:

$$\frac{\sigma(w)}{w} = \frac{\sigma_0 A}{\dot{\epsilon}_0^m} w^{m-1} = \frac{\sigma_0 A}{\dot{\epsilon}_0^m} |\dot{\epsilon}|^{m-1} \left[ \frac{\psi}{1-\theta} \left( \frac{\psi}{\phi} n^2 + 1 \right) \right]^{(m-1)/2}. \quad (13)$$

This paper is mainly devoted to studying the influence of both the Laplace pressure and the gas pressure in pores on the overall stress; for this reason, it is essential to monitor the magnitude  $|\sigma_z - p_L + p_I|$ , which can be regarded as a “driving force” of the sintering process, for each analyzed loading mode.

To this end, by substituting expression (13) into (11) the following relation can be obtained:

$$\sigma_z - p_L + p_I = \frac{A\sigma_0}{\dot{\epsilon}_0^m} |\dot{\epsilon}|^m \left[ \frac{\psi}{1-\theta} \left( \frac{\psi}{\phi} n^2 + 1 \right) \right]^{(m-1)/2} \left[ 1 + \sqrt{\frac{2}{3}} n \operatorname{sgn}(\dot{\epsilon}_z - \dot{\epsilon}_r) \right]^{-1/m}. \quad (14)$$

In order to achieve an analytical expression for the evolution of the material behavior during the sintering process, it is necessary now to introduce the porosity  $\theta$ , defined as the ratio of the volume of pores and the total volume. By denoting the total volume of the sintered material as  $V_{\text{tot}}$  and the volumes of the matrix pores as  $V_{\text{matrix}}$  and  $V_{\text{pores}} = V_{\text{tot}} - V_{\text{matrix}}$ , respectively, the relative density can be written as:

$$\rho = \frac{V_{\text{matrix}}}{V_{\text{tot}}}. \quad (15)$$

The porosity reads:

$$\theta = \frac{V_{\text{pores}}}{V_{\text{tot}}} = 1 - \rho. \quad (16)$$



Because of mass continuity and the assumed incompressibility of the matrix (the shrinkage is only due to the change of the porosity) [Olevsky 1998], the evolution law for the porosity is given by

$$\dot{\epsilon} = \frac{\dot{\theta}}{1-\theta}. \quad (17)$$

Taking into account expression (17) and recalling that the shrinkage is  $\dot{\epsilon} < 0$  and thus  $\dot{\theta} < 0$ , the relationship (14) leads to the following evolution equation for the porosity:

$$\begin{aligned} \dot{\theta} = & \operatorname{sgn}(\dot{\theta})[\operatorname{sgn}(\dot{\theta})(\sigma_z - p_L + p_I)]^{1/m} \frac{\dot{\epsilon}_0}{(A\sigma_0)^{1/m}} \\ & \times \left[ \frac{\psi}{1-\theta} \left( \frac{\varphi}{\psi} n^2 + 1 \right) \right]^{(1-m)/2m} \left[ \psi \left( 1 + \sqrt{\frac{2}{3}} n \operatorname{sgn}(\dot{\epsilon}_z - \dot{\epsilon}_r) \right) \right]^{-1/m} (1-\theta), \end{aligned} \quad (18)$$

which accounts for the contribution of the Laplace pressure and the gas pressure in the pores. The analogue of (18) neglecting such contributions was obtained in [Olevsky and Molinari 2006, Equation 15].

**2.1. Evolution law for porosity for isostatic pressing processes.** For the case of isostatic pressing,  $\sigma_z = \sigma_r$ ; in the sequel their common value will be denoted by  $\sigma$ . Here the loading mode parameter  $n$  is zero and the process entails a monotonic decrease of the porosity, that is,  $\dot{\theta} < 0$ ; hence, relation (18) reduces to the following expression:

$$\dot{\theta} = -[-(\sigma - p_L + p_I)]^{1/m} \frac{\dot{\epsilon}_0}{(A\sigma_0)^{1/m}} (1-\theta)^{(3m-1)/2m} \psi^{-(1+m)/2m}. \quad (19)$$

Obviously, since  $\dot{\gamma} = 0$ , the normalized shear modulus  $\varphi$  has no influence on the process. The normalized bulk modulus  $\psi$  is a known function of the porosity  $\theta$ ; for such a function, here and subsequently, we shall use the expressions given in Section 2.2. For this case, the models of [Ponte Castañeda 1991; Sofronis and McMeeking 1992] give the same behavior. This is because of the expression of the normalized bulk modulus  $\psi$ , which is indeed the same for both models.

Equation (19) may be normalized by using the dimensionless specific time defined as

$$\tau_L = \left[ \frac{p_{L0}}{\sigma_0 A} \right]^{1/m} \dot{\epsilon}_0, \quad (20)$$

where  $p_{L0}$  is the reference value of the Laplace pressure, dependent on the surface tension and on the characteristic radius of the particles; it will be discussed in Section 2.3. Consequently, the evolution law for the porosity (19) can be rewritten as

$$\frac{\partial \theta}{\partial \tau_L} = -(1-\theta)^{(3m-1)/2m} [-(\sigma - p_L + p_I)]^{1/m} \psi^{-(1+m)/2m}. \quad (21)$$

For future use, it is useful to introduce a dimensionless pressure parameter, called the specific external pressure (SEP):

$$\text{SEP} = \sigma/\alpha/r_0, \quad (22)$$

where  $\alpha$  denotes the surface tension and  $r_0$  the average radius of the particles (for further explanation, see Section 2.3).

**2.2. Dependence of the normalized shear and bulk moduli on porosity.** In the literature there are several studies relating to the determination of the normalized bulk and shear moduli. In particular we will use four different models:

- The Skorohod model [Skorohod 1972]:

$$\varphi = (1 - \theta)^2, \quad \psi = \frac{2}{3} \frac{(1 - \theta)^3}{\theta}.$$

- The Ponte Castañeda–Duva–Crow model [Ponte Castañeda 1991; Duva and Crow 1992]:

$$\varphi = \frac{(1 - \theta)^{2/(1+m)}}{1 + \frac{2}{3}\theta}, \quad \psi = \frac{2}{3} \left( \frac{1 - \theta^m}{m\theta^m} \right)^{2/(m+1)}.$$

- The McMeeking–Sofronis model [Sofronis and McMeeking 1992]:

$$\varphi = \left( \frac{1 - \theta}{1 + \theta} \right)^{2/(1+m)}, \quad \psi = \frac{2}{3} \left( \frac{1 - \theta^m}{m\theta^m} \right)^{2/(m+1)}.$$

- The Cocks model [Cocks 1994]:

$$\varphi = \frac{(1 - \theta)^{2/(1+m)}}{1 + \frac{2}{3}\theta}, \quad \psi = \frac{m + 1}{3} \frac{(1 + \theta)(1 - \theta)^{2/(m+1)}}{\theta}.$$

In Figures 2 and 3 moduli  $\psi$  and  $\varphi$ , respectively, are plotted as functions of porosity for different values of the parameter  $m$ . The Skorohod model accounts for linear-viscous incompressible material with voids only; indeed, the moduli  $\psi$  and  $\varphi$  are independent from the parameter  $m$ .

**2.3. Dependence of the Laplace pressure on porosity.** The effective Laplace pressure  $p_L$  is the result of the collective action of local capillary stresses in a porous material. A variety of approaches can be found in the literature. We will consider two possible derivations of the expression for the Laplace pressure.

(1) *Sintering stress derived by using a stochastic approach.* This derivation was employed by Skorohod [1972], who obtained  $p_L$  by calculating the surface free energy per unit mass with respect to the specific volume of the porous material by assuming spherical particles. The achieved result may be stated as follows:

$$p_L = p_{L0}(1 - \theta)^2 = \frac{3\alpha}{r_0}(1 - \theta)^2, \quad (23)$$

where  $\alpha$  is the surface tension and  $r_0$  is the characteristic radius of the particles.

(2) *Sintering stress derived by averaging the dissipation.* Here we summarize results shown in [Olevsky and Molinari 2000, Appendix A.2.2] about the derivation of an expression for the Laplace pressure. A hollowed sphere is considered as a schematic for a pore (see Figure 4); at its surface, namely for  $r = R_1$  (where  $r$  denotes the radial coordinate), the pressure  $p_{L0} = 2\alpha/r_0$  is applied, whereas the external boundary ( $r = R_2$ ) is stress free.

The porosity is then determined by the volume fraction:

$$\theta = \left( \frac{R_1}{R_2} \right)^3. \quad (24)$$

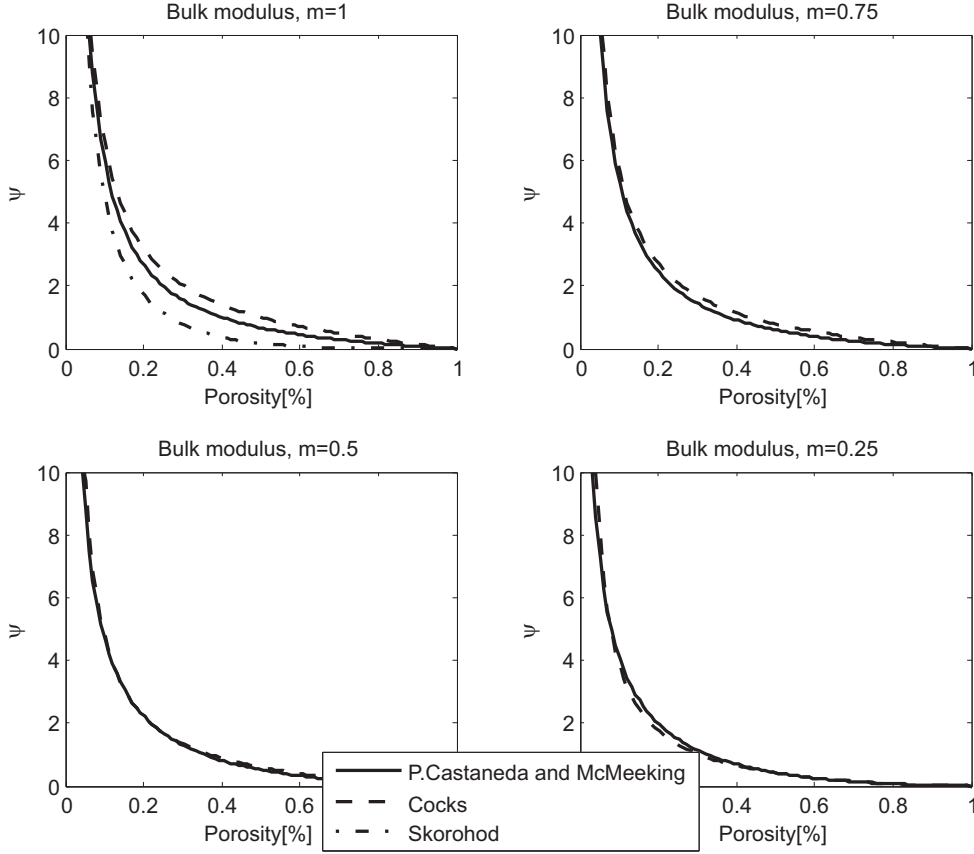


**Figure 2.** Normalized bulk modulus  $\psi$  as a function of porosity, for different values of the strain rate sensitivity,  $m$ .

The introduction of standard compatibility conditions into the constitutive relation (1) yields the radial and circumferential stresses as functions of the unknown radial velocity  $V_r(r)$  (and of  $p_L$  and  $p_I$ ). Finally, the stress balance (in the radial direction) allows for determining

$$V_r(r) = -\frac{p_{L0}R_1^3R_2^3}{2(A\sigma_0/\dot{\epsilon}_0^m)\varphi(R_2^3 - R_1^3)r^2}, \quad (25)$$

for  $m = 1$ , namely in the case of linearly viscous behavior.

Henceforth, the effective equivalent strain rate  $w$  (see (2)) appearing in (1) is relevant for the expression of the dissipation potential proposed in [Olevsky 1998, Equation (26)], that is,

$$D = \frac{A\sigma_0/(\dot{\epsilon}_0^{-1/m})}{m+1}(1-\theta)w^{m+1}. \quad (26)$$

Through this expression, the dissipation of the matrix and its average on the volume of the hollowed sphere may be deduced. Additionally, the dissipation of the effective porous material, subject to free sintering, is evaluated; its connection with the volume-averaged dissipation through Hill's identity [Olevsky

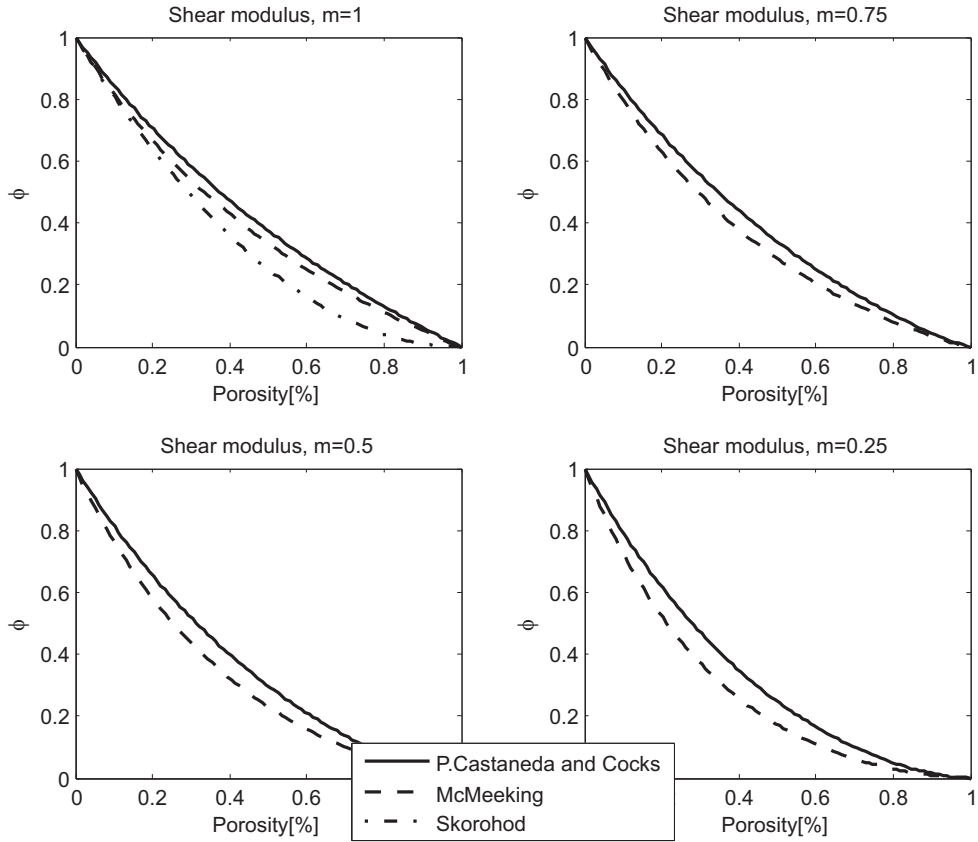


**Figure 3.** Normalized shear modulus  $\phi$  as a function of porosity, for different values of the strain rate sensitivity,  $m$ .

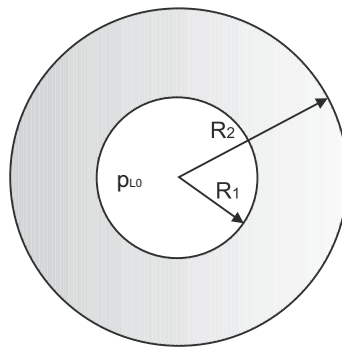


**Figure 4.** A representative element of the porous medium.

and Molinari 2000, Equation A29] allows for determining the following expression for the Laplace pressure:

$$p_L = \frac{2\alpha}{r_0} \sqrt{\frac{3}{2} \psi(\theta) \frac{\theta}{1-\theta}}. \quad (27)$$

The latter can be particularized to obtain the sintering stress associated with the models cited above; in particular,

- $p_L = \frac{2\alpha}{r_0}(1 - \theta)$  for the Skorohod model,
- $p_L = \frac{2\alpha}{r_0}$  for the Castañeda and McMeeking models, and
- $p_L = \frac{2\alpha}{r_0}\sqrt{1 + \theta}$  for the Cocks model.

Figure 5 shows the dependence of the Laplace pressure on the porosity  $\theta$ . The stochastic approach, yielding relation (23), gives a parabolic trend for the Laplace pressure. This is increasing when the porosity decreases and is independent of the value of the parameter  $m$ , so that  $p_L$  does not depend upon the material behavior. In particular, the values of pressure calculated through (27) are compatible enough with the ones obtained from (23) in the porosity range of interest for common sintered components (see the blown-up inset in Figure 5).

**2.4. Gas pressure in pores and its dependence upon porosity.** During the sintering process, the porosity becomes isolated and the final stage of sintering starts at a relative density  $\rho = 90\%$ , that is, at the closure porosity  $\theta_c = 0.1$ . At this time, the gas pressure in the pores is equal to the external pressure; as the relative density  $\rho$  increases, the gas pressure in the closed pores also increases. The more natural way to

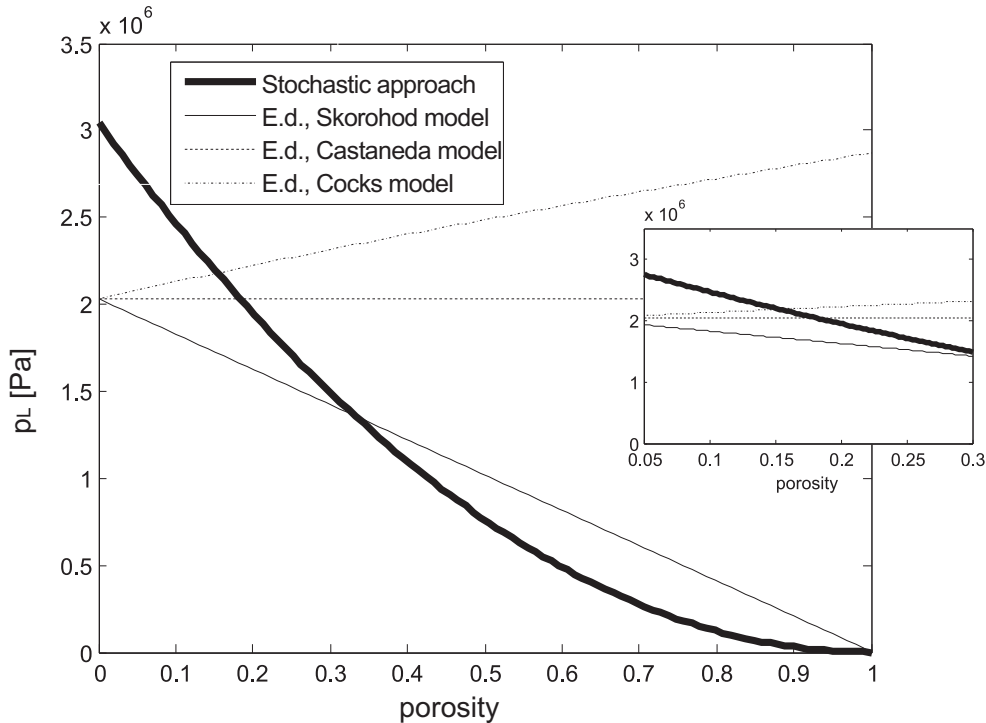


**Figure 5.** The Laplace pressure as a function of porosity.

account for such a phenomenon is through the ideal gas law [Arzt et al. 1983; Wilkinson 1988], that is,  $(p_I + p_{\text{atm}})V_{\text{pores}} = \text{const.}$ , where  $p_I$  is the gas pressure in the pores and  $p_{\text{atm}}$  the atmospheric pressure.

Recalling that, thanks to the incompressibility of the matrix,  $V_{\text{matrix}} = \text{const.}$  during the process, from the ideal gas law it follows that the quantity  $(p_I + p_{\text{atm}})(1 - \rho)/\rho = (p_I + p_{\text{atm}})V_{\text{pores}}/V_{\text{matrix}}$  remains constant. Recalling (16), the relationship can be rewritten as:

$$(p_I + p_{\text{atm}})\frac{\theta}{1-\theta} = \text{const.} = (p_0 + p_{\text{atm}})\frac{\theta_c}{1-\theta_c}, \quad (28)$$

where  $p_0$  is the external pressure (that is, the gas pressure in the pores when the porosity closes). Thus, the evolution of the pressure in the pores during the sintering process is given by

$$p_I = \begin{cases} 0, & \text{if } \theta > \theta_c, \\ (p_0 + p_{\text{atm}})\frac{\theta_c}{\theta} \frac{1-\theta}{1-\theta_c} - p_{\text{atm}}, & \text{if } \theta < \theta_c. \end{cases} \quad (29)$$

In the case of isostatic pressing, the external pressure is equal to the applied stress  $|\sigma|$ .

The effects of the Laplace pressure  $p_L$  and the gas pressure in the pores  $p_I$  are investigated in Sections 3 and 4, respectively.

### 3. Effect of the Laplace pressure on sintering processes entailing isostatic pressing

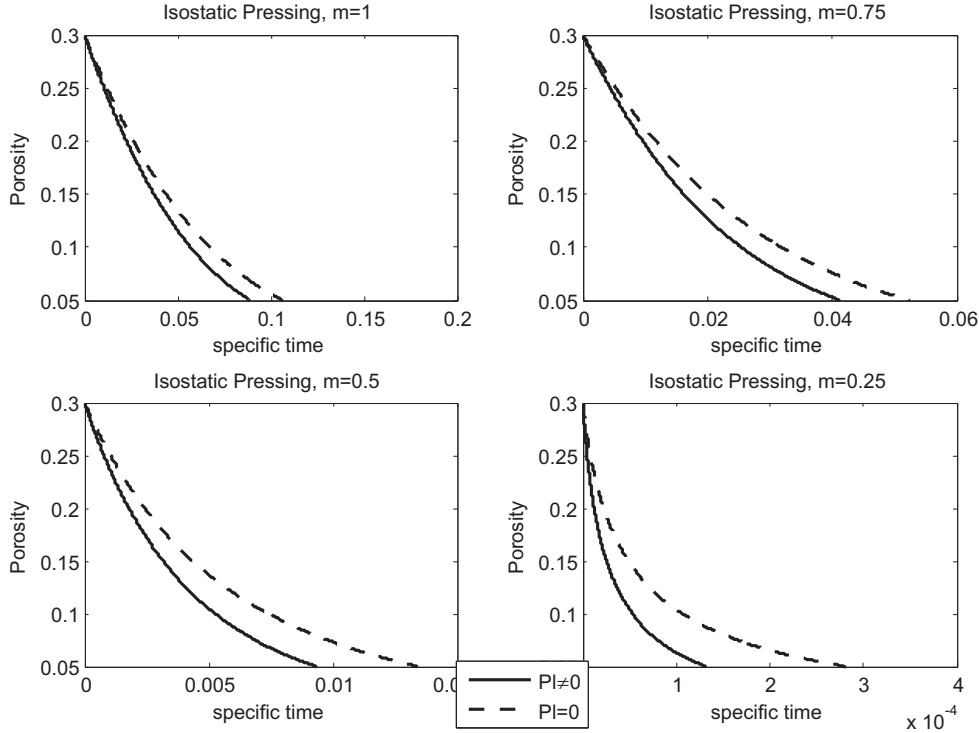
In this section, the effect of the Laplace pressure on sintering processes entailing isostatic pressing is studied. To be precise, processes entailing, as the driving force, only the stress due to the external load are compared to processes in which the Laplace pressure is taken into account.

Figure 6 shows the time evolution of the porosity during an isostatic pressing process that reduces the porosity from 30% to 5%, obtained by using the Castañeda–Duva–Crow model for  $\text{SEP} = 10$ , in two cases:

- Accounting for the interstitial pressure  $p_L$  (the continuous line), and the driving force of the process is  $\sigma - p_L$ .
- Neglecting the Laplace pressure (the dashed line), and the driving force is only the stress due to the external load,  $\sigma$ .

The latter describes the approximation adopted in [Olevsky and Molinari 2006]. Indeed, since  $|\sigma - p_L| > |\sigma|$ , the time decay of the porosity would be lower than in reality. Nevertheless, we record that the time evolution of the porosity has a qualitative analogue to the one obtained by neglecting  $p_L$  (see Figure 6). When the strain rate sensitivity,  $m$ , decreases, the initial part of both graphs become steeper. Indeed, for infinite slope, the material behavior would be perfectly plastic (this would correspond to  $m = 0$ ).

The gap between the two curves is higher for lower values of the strain rate sensitivity,  $m$ , hence the Laplace pressure has more influence on the sintering process when the material tends towards the plastic behavior. This may be explained by the (Ashby) power law (for example, (12)), relating the equivalent strain rate  $w$  and the effective equivalent stress  $\sigma(w)$ . Indeed, it is evident from such an equation that, for lower values of the strain rate sensitivity,  $m$ , the effective equivalent strain rate is more sensitive to stress changes, and, in particular, to the difference between the stress evaluated by accounting for the Laplace



**Figure 6.** Isostatic pressing: evolution of porosity for  $SEP = 10$ .

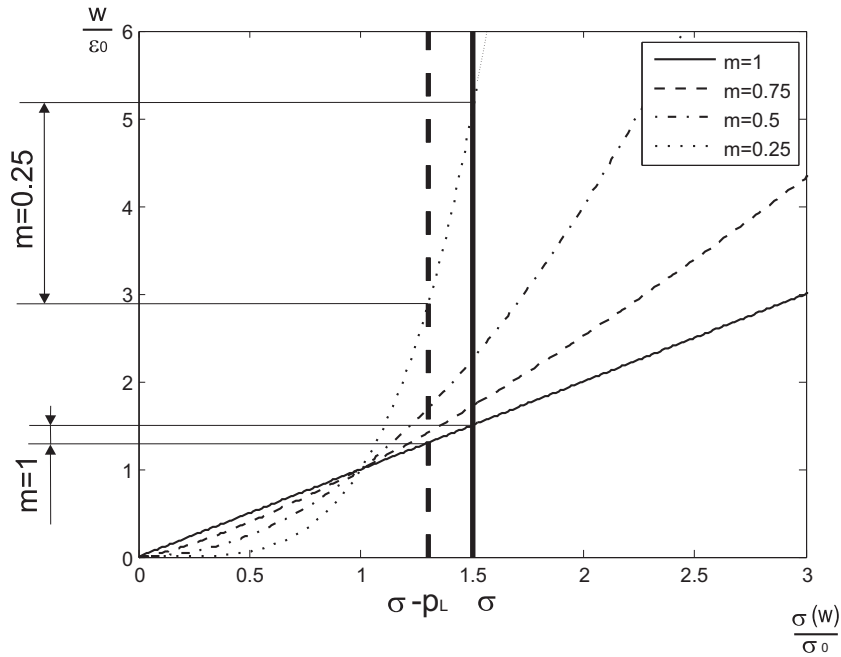
pressure as a driving force of sintering or by neglecting it. For the sake of clarity, the Ashby relation (12) is displayed in Figure 7 for different values of the parameter  $m$ ; the plot highlights the change of  $w$  obtained by considering as the driving force  $|\sigma - p_L|$  instead of  $|\sigma|$ , which is much more relevant for higher values of  $m$ .

Figure 8 is the analogue of Figure 6 for a lower value of external pressure, that is,  $SEP = 1$ . Here, the gap between the curves is remarkable because, in this case, the “sintering driving force” is basically the Laplace pressure, simply because it is higher than the externally imposed stress.

A comparison between the three different models for the normalized shear and bulk moduli  $\varphi$  and  $\psi$ , between the two different expressions for  $p_L$  (see (23) and (27)), is performed in the sequel. Figure 9 shows such a comparison for  $SEP = 5$ , for a material with linear-viscous behavior ( $m = 1$ ).

The time-evolution diagrams shown in the left and right parts of Figure 9 are similar, because the values of the Laplace pressure given by (23) and (27) are compatible enough for porosities between 30% and 5% (see the inset in Figure 5). The differences among the curves relative to the various considered models are due to the corresponding expressions of the normalized bulk modulus  $\psi$ .

**3.1. Influence of interstitial stress on industrial processes entailing isostatic pressing.** A specific metallic alloy (aluminum-zinc-magnesium-copper) is examined in this section. This is motivated by its extensive use in industrial sintering processes. The main features of this material are listed in Table 1. For aluminum alloys, the average sintering time is thirty minutes and usually the applied external pressure is on the order of 100 MPa [Muhlburger and Paschen 1993; Schaffer et al. 2001; Gokce and Findik 2008].



**Figure 7.** (Ashby) power law: sensitivity of the effective equivalent strain rate to the variation between  $\sigma$  and  $|\sigma - p_L|$ .

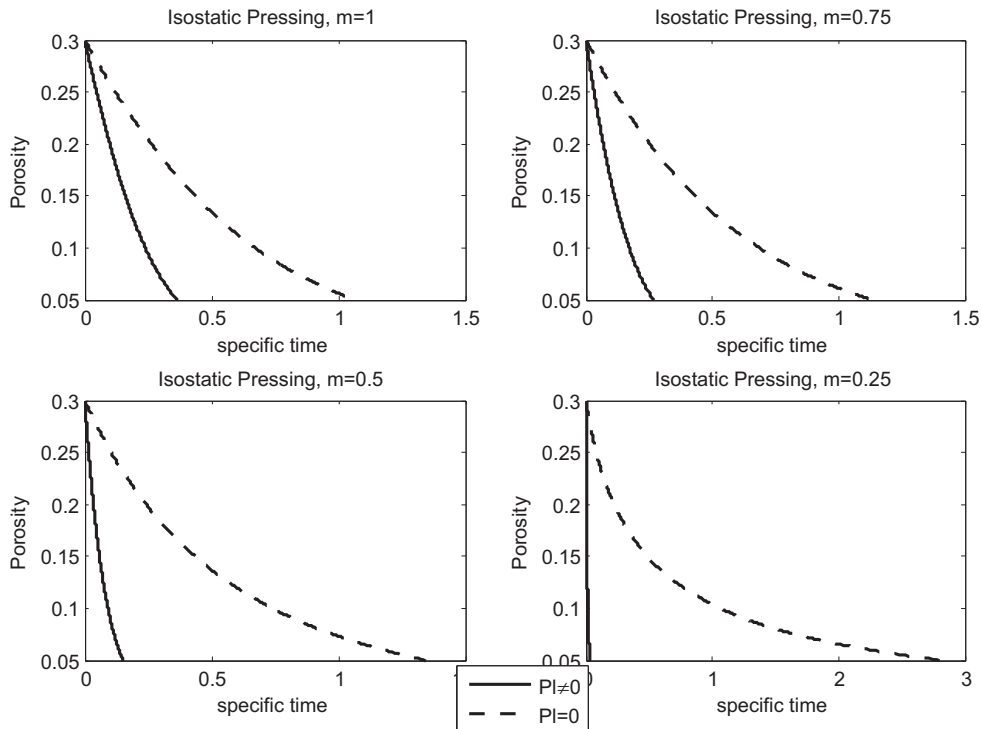


**Figure 8.** Isostatic pressing: evolution of porosity for  $SEP = 1$ .



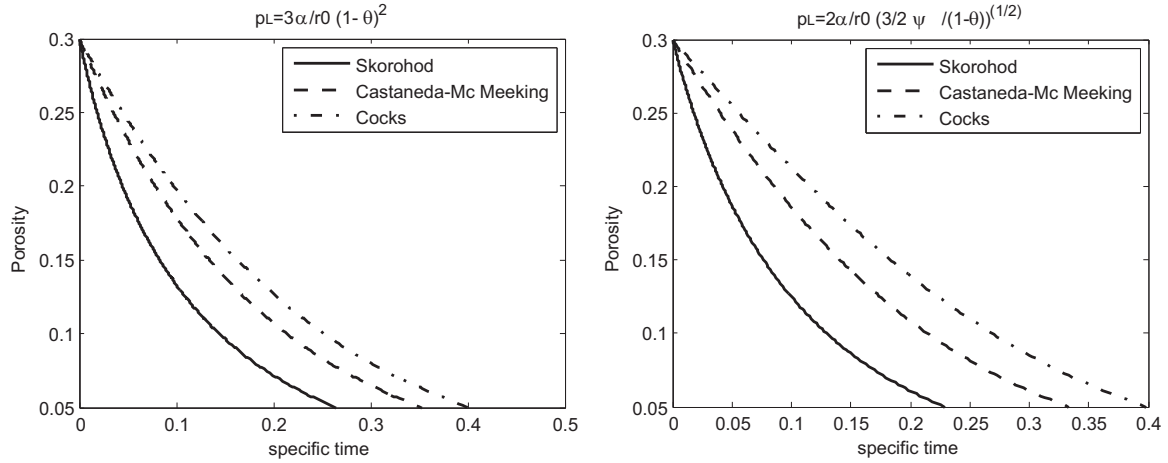


**Figure 9.** Isostatic pressing: evolution of porosity for  $SEP = 5$ ,  $m = 1$ , for different models.

It may be shown that the important parameters influencing the Laplace pressure are the radius of the grains,  $r_0$ , and the surface tension,  $\alpha$ . Values of the powder grain size from 20 nm to 5  $\mu\text{m}$  are taken into account here.

In the sequel, we shall examine the discrepancies in the estimates of the sintering times evaluated by either neglecting or accounting for the sintering stress  $p_L$ . Furthermore, we shall also calculate the residual porosity in both of the cases mentioned above.

**3.1.1. Threshold external loading pressures and sintering times.** Here we are interested in comparing the sintering times  $t$  and  $t_0$  employed to reduce the porosity from 30% to 5% in cases in which the sintering driving force is taken to be either  $|\sigma - p_L|$  or  $|\sigma|$ , respectively. We are also interested in calculating the values of the external pressure  $p^*$  for which the discrepancy between the sintering times, that is,  $(t - t_0)/t$ , attains the values 5%, 10%, and 15%. Obviously, whenever the external pressure is less than  $p^*$ , for a given value of discrepancy, for example 5%, an error greater than 5% occurs by neglecting the effect of the Laplace pressure.

Figures 10 and 11 show the threshold pressures for 5  $\mu\text{m}$  and 50 nm powders (obtained by the Castañeda model). We see immediately that the effect of the Laplace pressure becomes more relevant for

Young's modulus	$E$	70.7 GPa
Poisson's ratio	$\nu$	0.325
Surface tension	$\alpha$	1.128 N/m
Activation energy	$Q$	14390 kJ
Melting temperature	$T_m$	659° C
Average particle radius	$r_0$	5–50 $\mu\text{m}$
Sintering temperature	$T_s$	100–350° C
Sintering pressure	$P_b$	600–610 MPa

**Table 1.** Characteristics of the considered aluminum-zinc-magnesium-copper alloy.

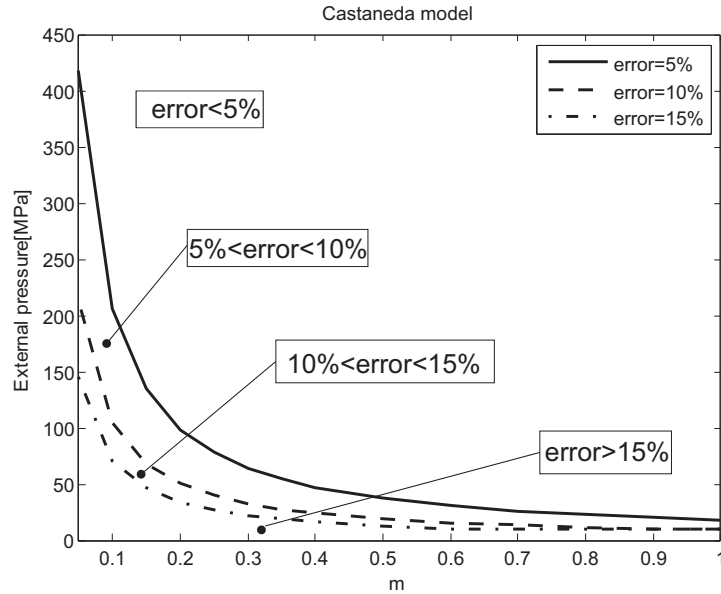


**Figure 10.** Threshold pressure  $p^*$ , for  $5 \mu\text{m}$  powder.

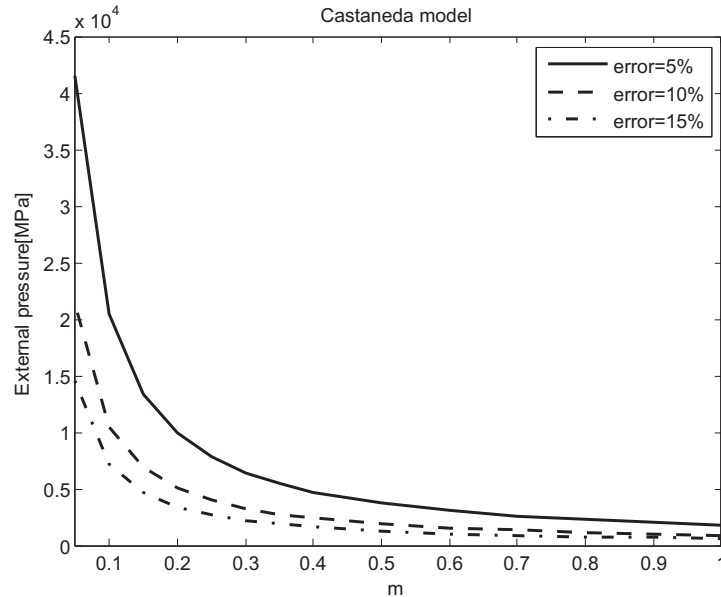


**Figure 11.** Threshold pressure  $p^*$ , for  $50 \text{ nm}$  powder.

lower values of the powder grain size. Hence, in this case the threshold pressures are comparable to those usually applied in industrial processes.

The threshold pressures evaluated by using the Cocks model do not exhibit meaningful differences with the results obtained by adopting the Castañeda model.

The results of these sections rely upon the model of the Laplace pressure based on the stochastic approach ((23), discussed in Section 2.3). Equation (27), instead derived by averaging the dissipation,

does not allow for evaluating  $p_L$  for different values of the strain rate sensitivity parameter  $m$ . However, the values of the threshold pressure obtained by using the latter model are in complete agreement with the ones obtained by using the former.

**3.1.2. Residual porosity.** The residual porosity is a fundamental feature of the material, because, among other reasons, it determines the mechanical properties of a sintered specimen.

A thirty-minute sintering process with external loading pressure of 100 MPa is now considered. Here we are interested in comparing the residual porosities  $\theta_r$  and  $\theta_{r0}$  after thirty minutes, when the sintering driving force is, respectively, taken to be either

- $|\sigma - p_L|$  or
- $|\sigma|$ .

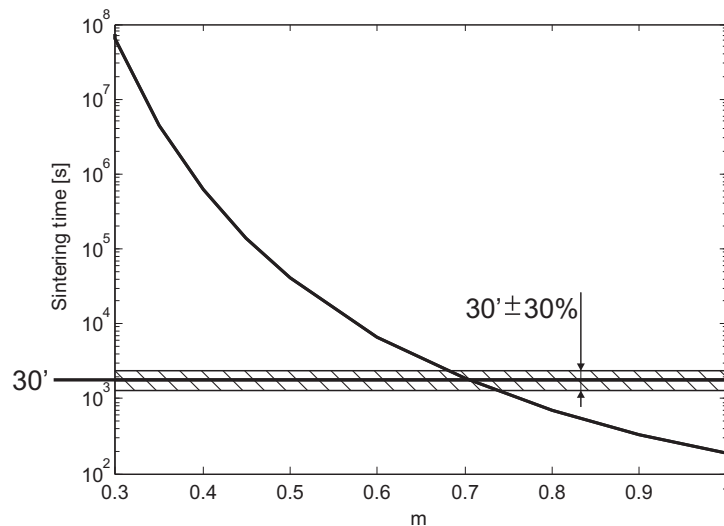
For the different values of powder grain size mentioned above, we are able to calculate the value of the strain rate sensitivity,  $m$ , that permits having a sintering reference time on the order of thirty minutes (30'). For the sake of convenience, without loss of generality, in the sequel a time range corresponding to a variation of  $\pm 30\%$  of the reference time is considered.

Figure 12 shows the sintering time (that is, the time required to reduce the porosity from 30% to 5%) as a function of the strain rate sensitivity,  $m$ ; furthermore, the values of  $m$  corresponding to the real sintering times of  $30' \pm 30\%$  are highlighted in the plot.

With such values of the parameter  $m$ , we may calculate the percentage error

$$E\% = \frac{\theta_r - \theta_{r0}}{\theta_r} 100[\%], \quad (30)$$

occurring when the Laplace pressure,  $p_L$ , is neglected. Figure 13 shows value of such an error as a function of the strain rate sensitivity,  $m$ , for grain sizes between 20 nm and 1  $\mu\text{m}$ .



**Figure 12.** Sintering time as a function of the strain rate sensitivity,  $m$ .

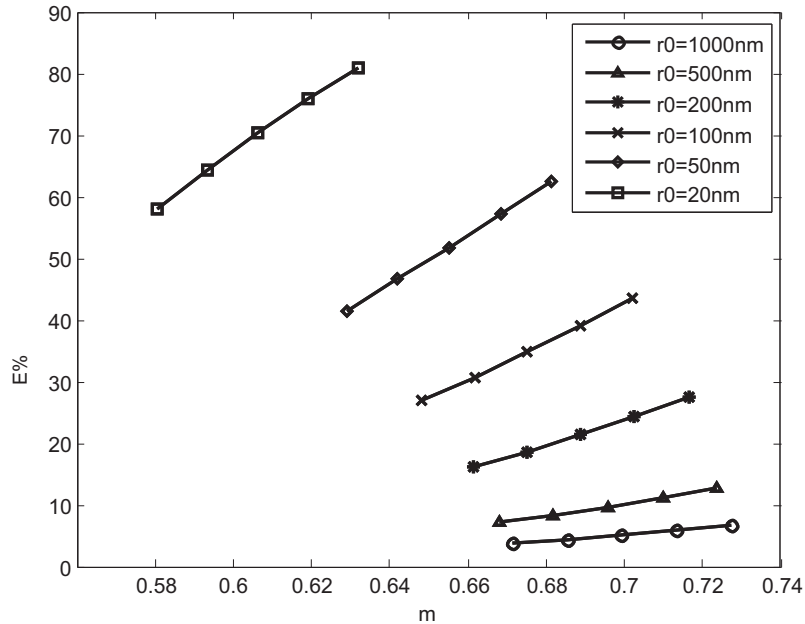


**Figure 13.** Errors  $E\%$  on the residual porosity for different values of the grain size,  $r_0$ .

For nanopowders (that is, for grain sizes less than  $1 \mu\text{m}$ ) the error becomes much higher than in the case of micropowders. In particular, for sizes on the order of  $100 \text{ nm}$  an error of about  $40\%$  may occur, while for  $20 \text{ nm}$  the error is on the order of  $80\%$ . For lower grain sizes, the gap between  $\theta_r$  and  $\theta_{r_0}$  is higher than for the previous cases.

The second parameter influencing the Laplace pressure is the surface tension  $\alpha$ ; there are lots of uncertainties in the determination of its value [Kumikov and Khokonov 1983]. Hence, because of the lack of reliability, the sensitivity of the model to variations of  $\alpha$  in the range of  $\pm 50\%$  is analyzed. Figure 14 shows the error  $E\%$  (defined by (30)) as a function of the surface tension  $\alpha$ , for different values of the powder grain size. For increasing values of  $\alpha$ , the Laplace pressure grows and hence the gap between  $\theta_r$  and  $\theta_{r_0}$  increases accordingly; this phenomenon turns out to be more relevant for lower powder grain sizes.

#### 4. Effect of the gas pressure in pores on sintering processes entailing isostatic pressing

In this section the effect of the gas pressure in pores on sintering processes entailing isostatic pressing is studied through the comparison of results obtained by accounting for  $p_I$  or by neglecting it. Isostatic pressing processes that reduce the porosity from  $30\%$  to  $5\%$  are considered. The evolution of the pressure in the pores during sintering is given by (29) where, in the case of isostatic pressing, the external pressure  $p_0$  is equal to the absolute value  $|\sigma|$  of the applied stress.

Figure 15 shows, for  $\text{SEP} = 10$ , the absolute values of the *sintering driving forces*, that is, the stress due to the external load, the gas pressure in the pores, and the Laplace pressure. Figure 16 shows the values of the total sintering driving force, for different values of the SEP, in two cases:

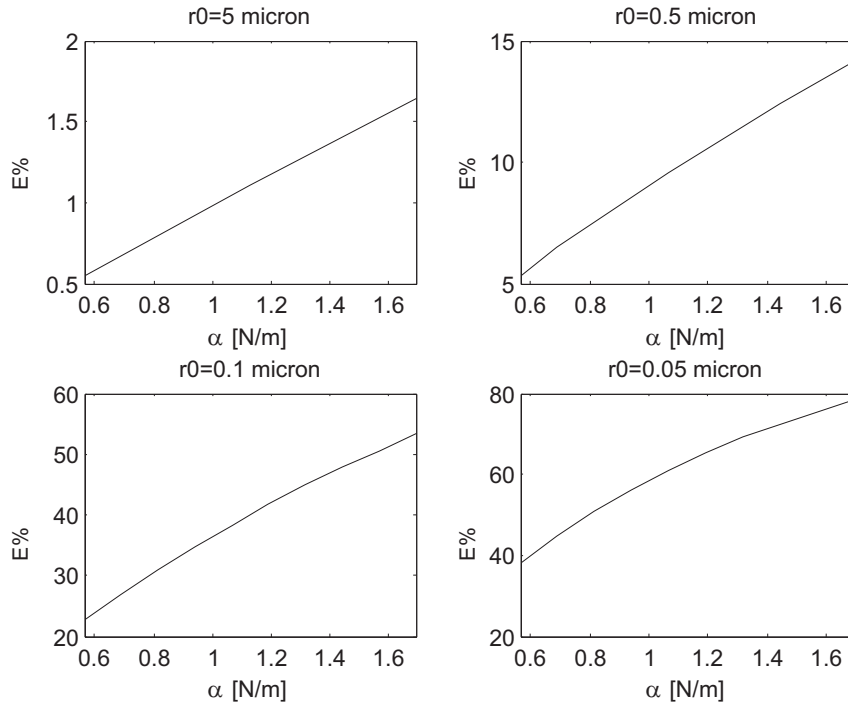


**Figure 14.** Errors  $E\%$  on the residual porosity, for different values of the surface tension,  $\alpha$ .

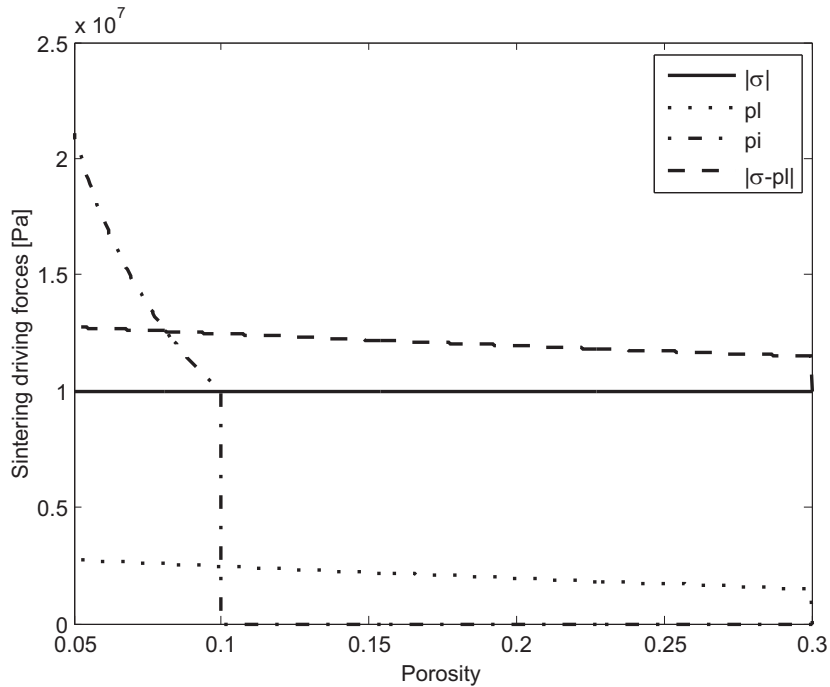


**Figure 15.** Sintering driving forces.

- accounting for the whole driving force (the dashed line)  $\sigma - p_L + p_I$  and
- neglecting the gas pressure in the pores (the dotted line), that is, the driving force is considered to be  $\sigma - p_L$ .

The latter describes nonpressurized pores. Indeed, since no pressure could act against stresses caused by external loading (and Laplace pressure), the time decay of the porosity, in this case, would be faster than in reality. It is noticeable that, since  $\sigma - p_L < 0$  and  $p_I \geq 0$  during the whole sintering process (see (29)), the total driving force  $\sigma - p_L + p_I$  may turn out to become null at a definite value of the porosity. Such a value will be denoted by  $\theta^*$  and be given by the following condition:

$$|\sigma - p_L(\theta^*)| = p_I(\theta^*). \quad (31)$$

In the limiting case for which condition (31) holds, (21) yields  $\dot{\theta} = 0$  and hence  $\theta = \text{const}$ . Thus, whenever such a condition is achieved the porosity remains constant at the limit value  $\theta^*$ .

It is evident that the value of  $\theta^*$  depends upon the external load and the choice of expression (23) or (27) for the Laplace pressure. Moreover, since  $p_I = 0$  for  $\theta > \theta_c$ , condition (31) can be verified only in the third phase of sintering, when  $p_I > 0$ ; it leads to  $\theta^* < \theta_c$ .

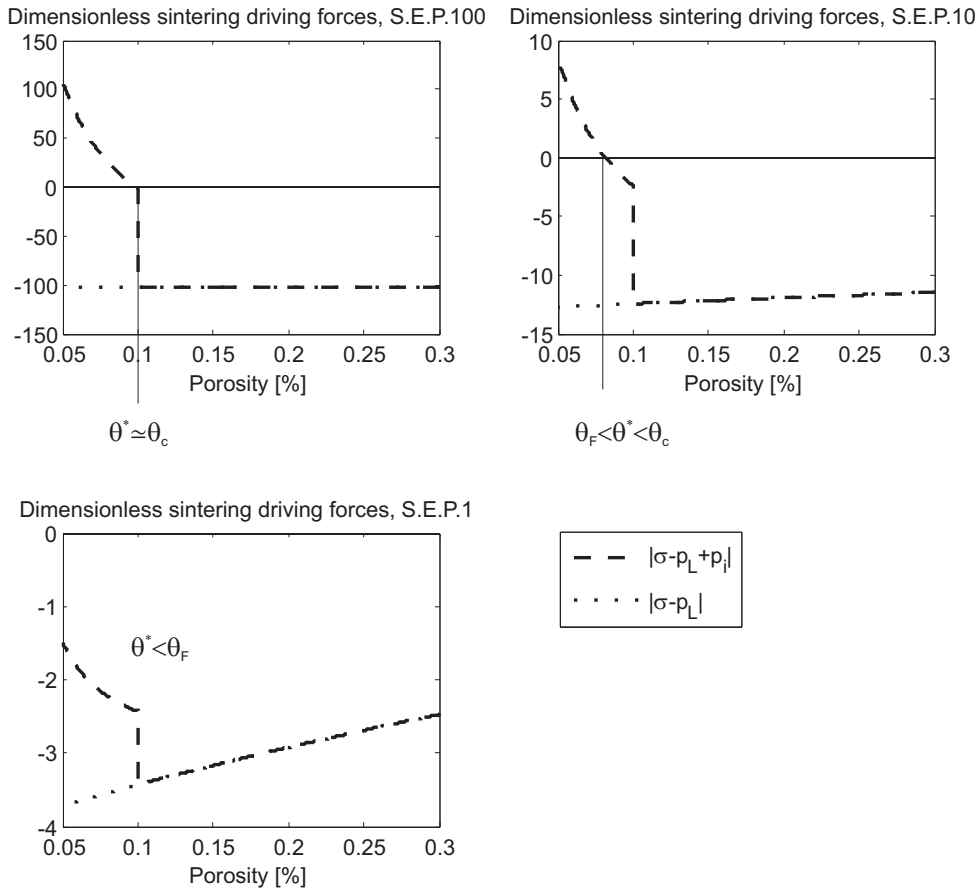


**Figure 16.** Dimensionless total sintering driving forces.

By denoting with  $\theta_F$  the desired porosity at the end of the process and recalling that  $\theta_c$  denotes the closure porosity, that is, the value of the porosity for which the pores becomes isolated, we may now distinguish two cases:

- *Case in which  $\theta_F < \theta^* < \theta_c$ .* Figure 17 shows the time evolution of the porosity, obtained by using the Castañeda–Duva–Crow model, for different values of the strain rate sensitivity,  $m$ , for  $SEP = 10$ , in two cases:
  - accounting for the gas pressure in the pores  $p_I$  (the continuous line), and
  - neglecting this pressure (the dashed line).

It is evident that, since  $\theta > \theta_c$  (that is, during the first and second phases of sintering), the evolution of the porosity obviously is not affected by the presence of  $p_I$ , and hence the curves coincide. When the third phase begins, at porosity  $\theta = \theta_c$ , the dashed line moves away from the continuous one; as stated above, the sintering time obtained by accounting for the gas pressure in the pores is higher than the one obtained by neglecting it.

The fundamental result, in the case under examination, is that the desired final value of the porosity  $\theta_F$  cannot be obtained; the value of the porosity at the end of the process is given by  $\theta^* > \theta_F$ . Moreover, whenever the condition (31) is achieved the rate of change of the porosity goes to zero; in the proximity of such a condition, the time-porosity graph presents an horizontal plateau.

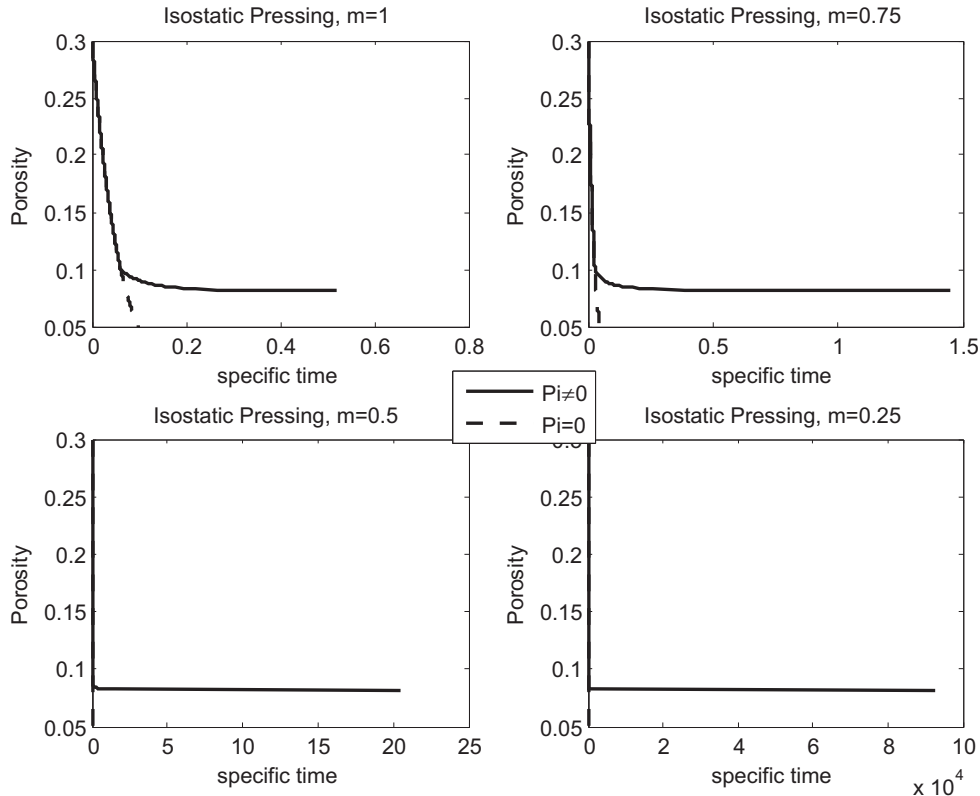


**Figure 17.** Isostatic pressing: evolution of porosity for  $SEP = 10$ .

This leads to a stretch of sintering times, which is evident from Figure 17.

- *Case in which  $\theta^* < \theta_F$ .* Figure 18 shows the time evolution of the porosity, obtained by using the Castañeda–Duva–Crow model, for different values of the strain rate sensitivity,  $m$ , for  $SEP = 1$ . It is evident from Figure 16 that, for such a value of the SEP, the critical porosity  $\theta^*$  is not achieved in the range of the considered porosities, that is,  $\theta^* < \theta_F$ . This allows for obtaining the desired porosity  $\theta_F$  at the end of the process. The only effect of the gas pressure in the pores is to stretch the sintering times. This phenomenon will be studied in the following subsection.

In both cases, the gap between the two curves is higher for lower values of the strain rate sensitivity,  $m$ , and hence the presence of gas pressure in the pores has more influence on the sintering process whenever the material tends towards the plastic behavior. This may be explained by the (Ashby) power law (12), that indicates that for lower values of the parameter  $m$ , the effective equivalent strain rate is more sensitive to stress changes.

Comparison between the three different models for the normalized shear and bulk moduli  $\varphi$  and  $\psi$  and between the two different expressions for  $p_L$  (see (23) and (27)) is performed in the sequel. Figure 19 shows such a comparison for  $SEP = 1$  for a material with linear-viscous behavior ( $m = 1$ ).

The time-evolution diagrams shown in the left and right portions of Figure 19 are quite similar, because the value of the Laplace pressure given by (23) and (27) are compatible enough for porosities

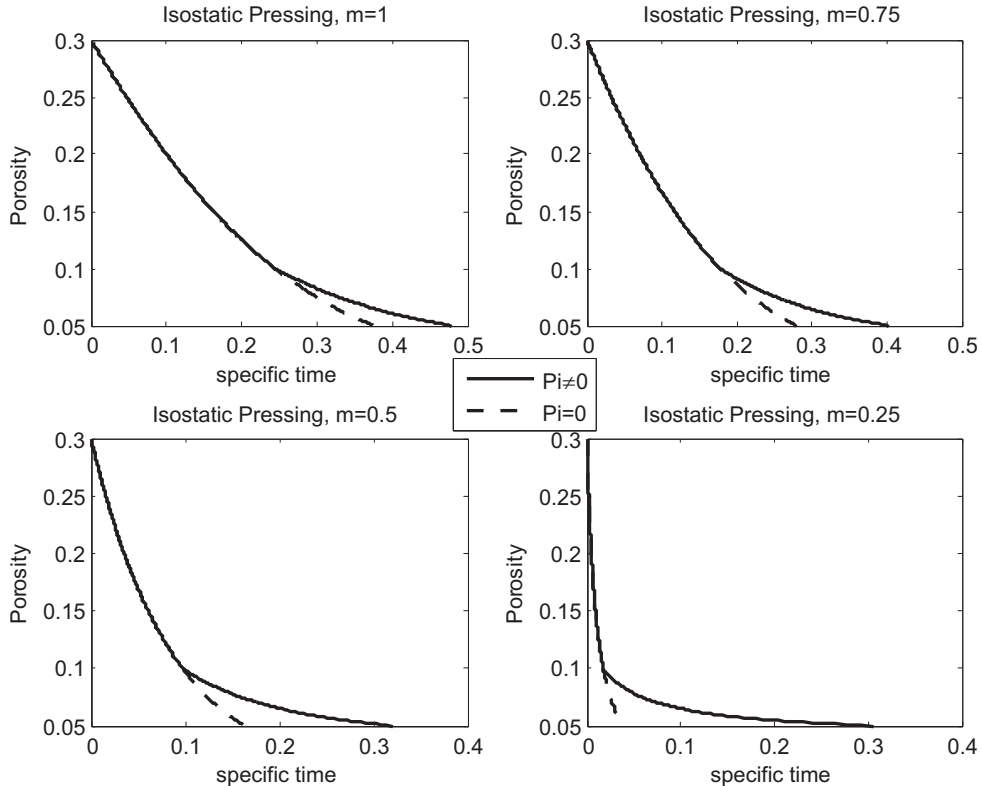


**Figure 18.** Isostatic pressing: evolution of porosity for  $SEP = 1$ .



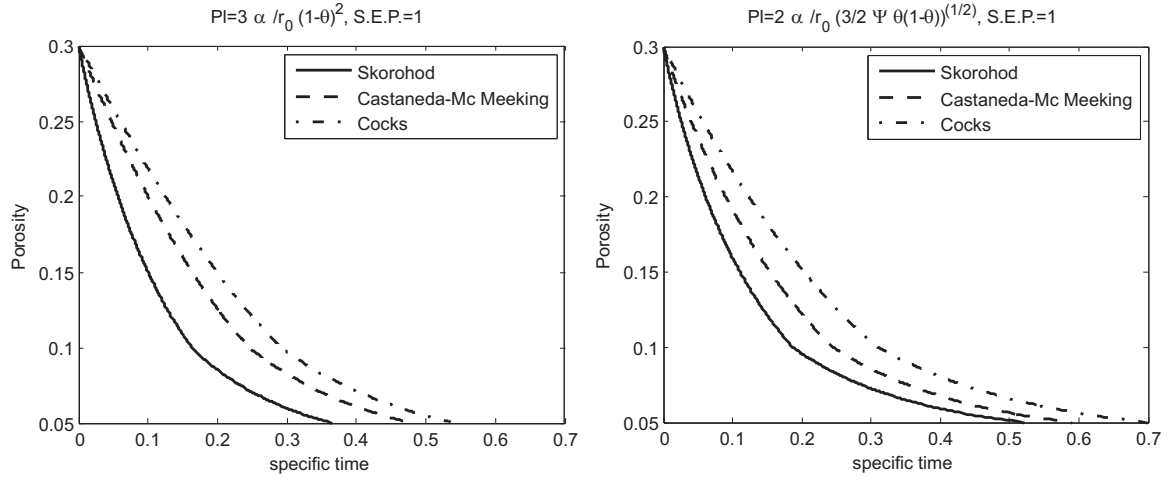


**Figure 19.** Isostatic pressing: evolution of porosity for SEP = 1.

between 30% and 5% (see the inset in Figure 5). The differences among the curves relative to the various considered models are due to the corresponding expressions of the normalized bulk modulus  $\psi$ .

Figure 20 shows such a comparison for SEP = 10 with  $m = 1$ . In this case as well, the left and right-hand graphs are similar. The differences among the curves relative to the various considered models are due to the corresponding expressions of the normalized bulk modulus  $\psi$ , leading, in the case of  $p_L$  given by (27), to slightly different values of the critical porosity  $\theta^*$ .

**4.1. Influence of the gas pressure in pores on industrial processes entailing isostatic pressing.** Similarly to the analysis performed in Section 3.1, we are interested in determining if there exists a threshold for the external pressure under (or over) which the effect of the gas pressure in pores is negligible in a “real” industrial process. The same aluminum-zinc-magnesium-copper alloy presented in Section 3.1 is considered here.

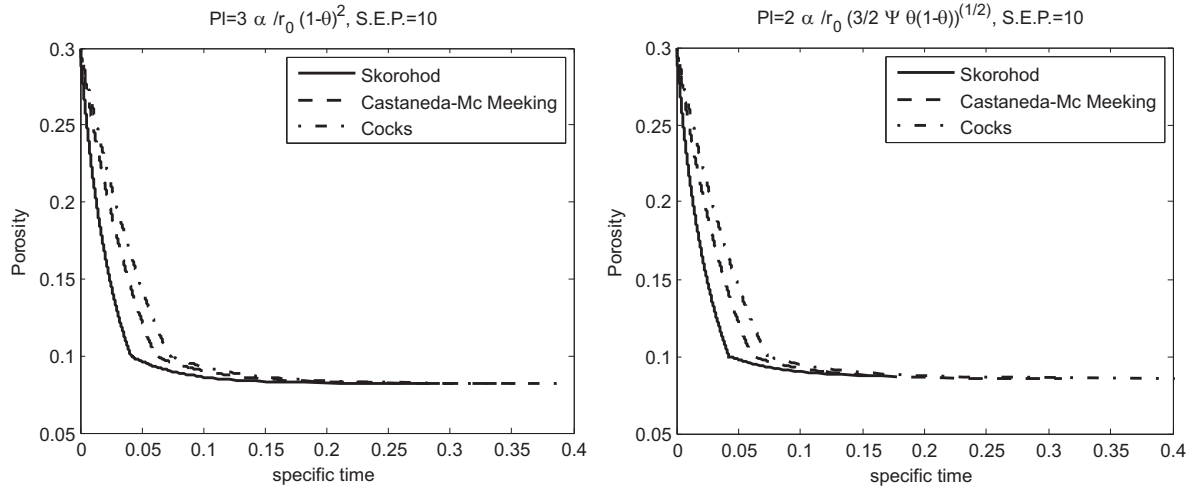


**Figure 20.** Isostatic pressing: evolution of porosity for SEP = 10.

As discussed above, in the case of isostatic pressing, the gas pressure in the pores at the beginning of the third phase of sintering (that is, at the closure porosity,  $\theta_c$ ) is equal to the external pressure. Hence, whenever the external pressure increases, the pressure in the pores also increases, acting “against” the sintering process and preventing the desired final porosity from being reached. Figure 21 shows the final porosity that can be reached as a function of the applied external pressure for different values of the strain rate sensitivity,  $m$ , for both  $5 \mu\text{m}$  and  $50 \text{ nm}$  powders.

Since the required final porosity can be reached only for low values of the external pressure (and, hence, of the gas pressure in the pores), there is no sense in looking for an external pressure threshold under which the effect of the gas pressure in the pores is negligible from the point of view of the sintering time, or the error on the evaluation of the residual porosity, similarly to Sections 3.1.1 and 3.1.2.

## 5. Stability

**5.1. Lower-order analysis.** Here we may denote by  $\theta^{(0)}(t)$  the fundamental solution of the evolution law (19) associated with a uniform distribution of the initial porosity. Following [Olevsky and Molinari 2006, §3.1.1] we assume that the perturbed solution has the form

$$\theta(t) = \theta^{(0)}(t) + \delta\theta(t) \exp(\lambda(t - t_0)), \quad (32)$$

where the magnitude of the perturbation  $\delta\theta(t)$  is taken to be much smaller than that of  $\theta^{(0)}(t)$  at all times. In [Olevsky and Molinari 2006, §3.1.1] a normalized perturbation growth rate with respect to the current rate of change of porosity is considered; this is done in order to have “first”-order information about the stability of the process. The quantity  $\lambda = \delta\dot{\theta}/\delta\theta$  can be regarded as the perturbation growth rate. It is possible to calculate the quantity  $\lambda/\dot{\theta}$  as a function of  $\theta$ ,  $\theta_0$ ,  $m$ ,  $p_L$ , and the external pressure. This can be done in the framework of the three different models considered in the previous sections.

Because, during sintering, shrinkage occurs monotonically ( $\dot{\theta} \leq 0$ ), the problem is linearly stable if  $\lambda < 0$ , that is,  $\lambda/\dot{\theta} > 0$ , while it is linearly unstable if  $\lambda > 0$ , that is,  $\lambda/\dot{\theta} < 0$ . In Figure 22 the quantity

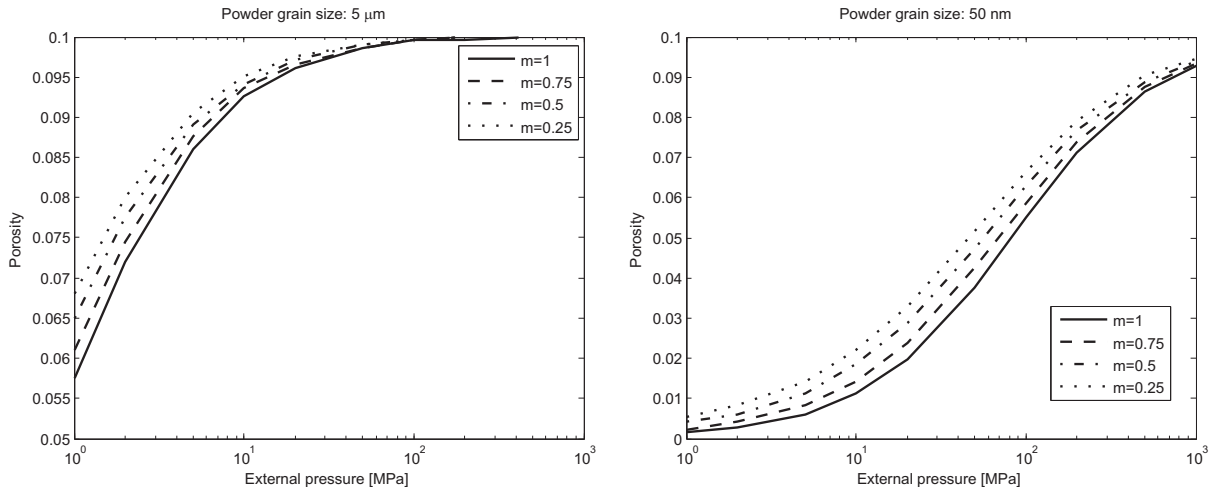


**Figure 21.** Final porosity as a function of applied external pressure, for  $5 \mu\text{m}$  powder.

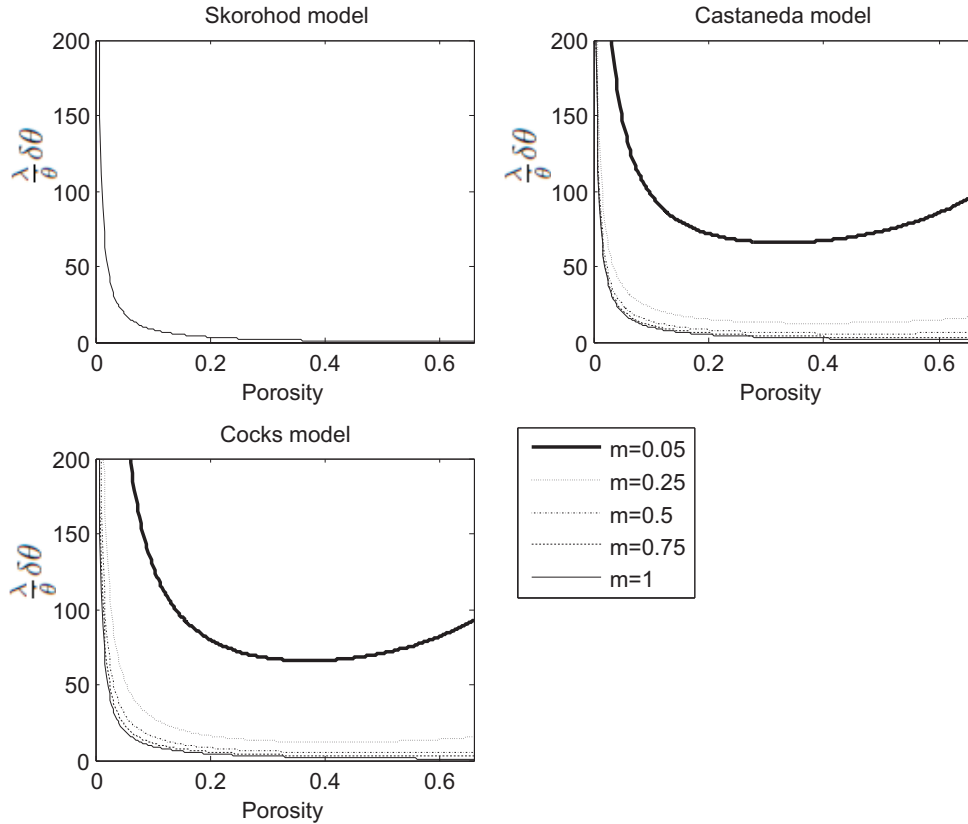


**Figure 22.** Normalized perturbation growth rate. Low order,  $SEP = 10$ .

$(\lambda/\dot{\theta})\delta\theta$  is plotted as a function of  $\theta$  for different values of the strain rate sensitivity,  $m$ , with  $SEP = 10$ . It is evident from the graph that the process is always linearly stable. The value of the applied external pressure does not change the stability condition.

**5.2. Higher-order analysis: Effect of the Laplace pressure.** The former analysis was meant to explore the consequences of the perturbation of the porosity on the rate of change  $\dot{\theta}$ , evaluated by (19).

In the present context the stress  $\sigma$  is uncoupled from porosity, hence a more refined method of producing perturbations is needed. To this end, one may follow the procedure used in [Olevsky and Molinari 2006, §3.1.2] to account for perturbation of the actual porosity and, in our case, of the Laplace pressure. Note that the quantity  $p_{L0}$  (which can be written as a function of  $p_L$  and the porosity through (23) or (27)) is a material property and does not change during the sintering process.

Two differences may be highlighted between the stability analysis performed in the present work and the one introduced in [Olevsky and Molinari 2006]:

- Unlike in [Olevsky and Molinari 2006], here the high-order analysis entails a process with constant external pressure.
- The presence and the perturbation of the sintering stress  $p_L$  is considered here.

A perturbed solution is considered in the following form:

$$\theta(t) = \theta^{(0)}(t) + \delta\theta \exp(\lambda(t - t_0)), \quad p_L(t) = p_L^{(0)}(t) + \delta p_L \exp(\lambda(t - t_0)); \quad (33)$$

by substituting (33) in (19) and (23) (for the Laplace pressure derived by using stochastic approach), after linearization about the fundamental solution  $(\theta^{(0)}(t), p_L^{(0)})$  we have

$$\begin{bmatrix} \frac{1}{\dot{\theta}} \frac{\partial f(\theta, \sigma, p_L)}{\partial \theta} - \frac{\lambda}{\dot{\theta}} & \frac{1}{\dot{\theta}} \frac{\partial f(\theta, \sigma, p_L)}{\partial p_L} \\ \frac{\partial p_{L0}(\theta, p_L)}{\partial \theta} & \frac{\partial p_{L0}(\theta, p_L)}{\partial p_L} \end{bmatrix}_{\theta^{(0)}(t), p_L^{(0)}(t)} \begin{bmatrix} \delta\theta \\ \delta p_L \end{bmatrix} = \begin{bmatrix} 0 \\ 0 \end{bmatrix}, \quad (34)$$

where

$$f(\theta, \sigma, p_L) = \dot{\epsilon}_0 (1 - \theta)^{(3m-1)/2m} \left( \frac{|\sigma_z - p_L|}{A\sigma_0} \right)^{1/m} \psi^{-(1+m)/2m}, \quad (35)$$

and where the matrix in (34) is evaluated at  $(\theta^0(t), p_L^0(t))$ , as specified. Equation (34) has nontrivial solutions if and only if the determinant of the matrix is equal to zero. By imposing this condition, we obtain a characteristic first-order equation with respect to the normalized perturbation growth rate  $\lambda/\dot{\theta}$ . As in the lower-order case, the quantity  $\lambda = \delta\dot{\theta}/\dot{\theta}$  can be regarded as the perturbation growth rate. Since, during sintering, shrinkage occurs monotonically ( $\dot{\theta} \leq 0$ ), the problem is linearly stable if the quantity  $\lambda/\dot{\theta}$  (the normalized perturbation growth rate) is negative, and linearly unstable if  $\lambda/\dot{\theta} > 0$ . This can be done in the framework of the three different models considered in the previous sections.

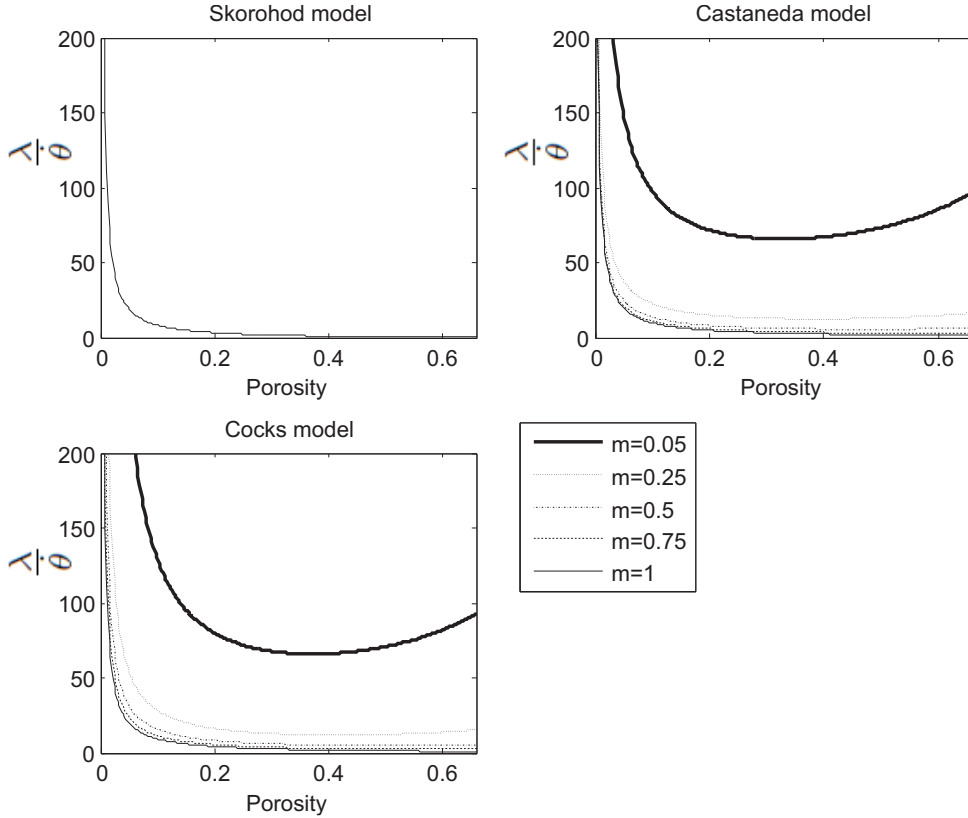
The root of (34) is shown in Figure 23 for the three principal cases defined in Section 2.1. It is evident that, since the normalized perturbation growth rate  $\lambda/\dot{\theta}$  is negative for the whole porosity range, the sintering process is always stable. By carefully comparing Figure 22 to Figure 23 it can be detected that the effect of the Laplace pressure is to slightly increase the absolute value of  $\lambda/\dot{\theta}$ , that is, to increase the stability of the process.

Figure 23 shows the results obtained considering the Laplace pressure evaluated by using the stochastic approach, leading to expression (23) for the sintering stress. The results obtained by using the other methodology (which leads to  $p_L$  given by (27)) are very similar.

**5.3. Higher-order analysis: Effect of the gas pressure in the pores.** In this subsection, perturbations of the porosity evolution rate, Laplace pressure, and gas pressure in the pores,  $p_I$ , are introduced, in order to investigate the effect of  $p_I$  on the stability of the sintering process. Such perturbations are considered in the following form:

$$\begin{aligned} \theta(t) &= \theta^{(0)}(t) + \delta\theta \exp(\lambda(t - t_0)), \\ p_L(t) &= p_L^{(0)}(t) + \delta p_L \exp(\lambda(t - t_0)), \\ p_I(t) &= p_I^{(0)}(t) + \delta p_I \exp(\lambda(t - t_0)). \end{aligned} \quad (36)$$

The latter is substituted in the governing equations of the problem, namely (19), (29), and (23) (for the Laplace pressure derived by using stochastic approach) or (27) (for Laplace pressure obtained through dissipative approach). Note that the external pressure at the pore closure,  $p_0$ , is a fixed parameter. After a linearization about the fundamental solution  $(\theta^{(0)}(t), p_I^{(0)}, p_L^{(0)})$ , the following set of equations can



**Figure 23.** Normalized perturbation growth rate. High-order stability analysis, SEP = 10.

be obtained:

$$\begin{bmatrix} \frac{1}{\dot{\theta}} \frac{\partial f(\theta, \sigma, p_L)}{\partial \theta} - \frac{\lambda}{\dot{\theta}} & \frac{1}{\dot{\theta}} \frac{\partial f(\theta, \sigma, p_L)}{\partial p_L} & \frac{1}{\dot{\theta}} \frac{\partial f(\theta, \sigma, p_L)}{\partial p_I} \\ \frac{\partial p_{L0}(\theta, p_L)}{\partial \theta} & \frac{\partial p_{L0}(\theta, p_L)}{\partial p_L} & 0 \\ \frac{\partial p_0(\theta, p_I)}{\partial \theta} & 0 & \frac{\partial p_0(\theta, p_I)}{\partial p_I} \end{bmatrix}_{\theta^{(0)}(t), p_L^{(0)}(t), p_I^{(0)}(t)} \begin{bmatrix} \delta\theta \\ \delta p_L \\ \delta p_I \end{bmatrix} = \begin{bmatrix} 0 \\ 0 \\ 0 \end{bmatrix}. \quad (37)$$

As in the previous subsection, in order to obtain nontrivial solutions of (37), the determinant of the matrix has to be null. By imposing such a condition, a first-order equation with respect to the normalized perturbation growth rate  $\lambda/\dot{\theta}$  is obtained. As in the previous cases, the problem is linearly stable if the quantity  $\lambda/\dot{\theta}$  (normalized perturbation growth rate) is negative, and linearly unstable if  $\lambda/\dot{\theta} > 0$ . The normalized perturbation growth rate is plotted in Figure 24 as a function of the porosity, for different values of  $m$  and for the Skorohod, Castañeda–McMeeking, and Cocks models. Obviously, the presence of  $p_I$  influences just the third phase of the sintering process, for relative densities greater than 90%, that is, for  $\theta < \theta_c = 0.1$ . Moreover, the final porosity  $\theta^*$  is here greater than zero, and depends upon the applied external pressure.

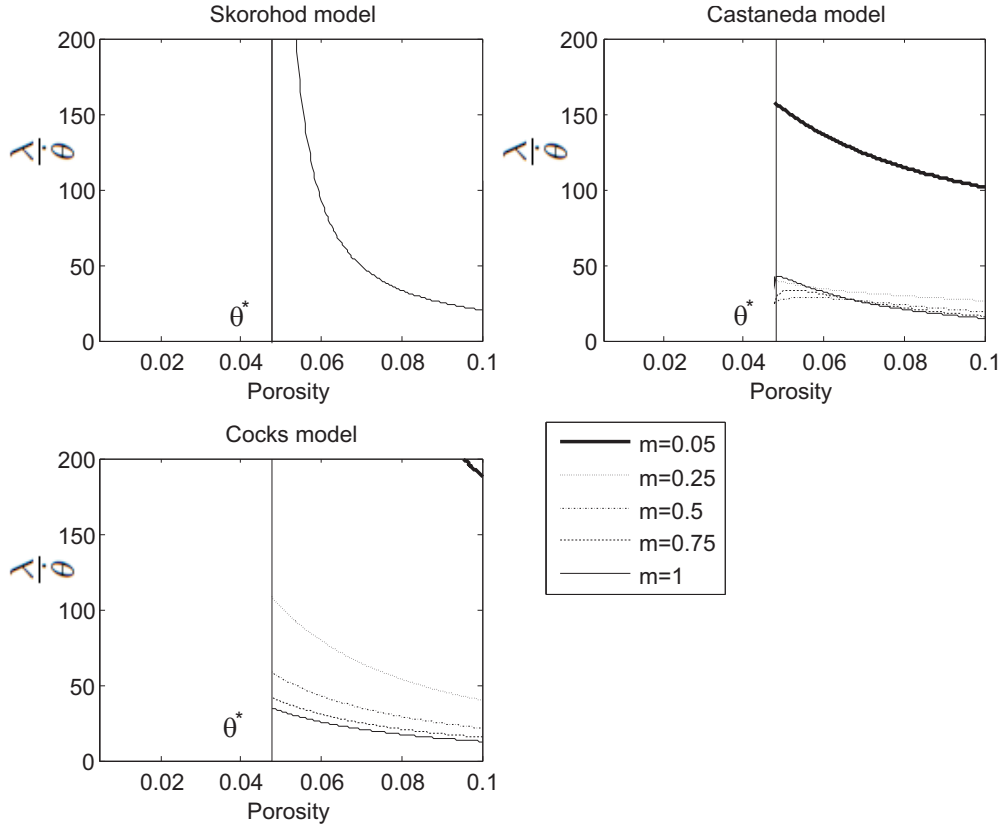


**Figure 24.** Normalized perturbation growth rate. High-order stability analysis,  $SEP = 2$ .

As it is evident from Figure 24, the effect of the gas pressure in the pores is to reduce the value of the normalized perturbation growth rate  $\lambda/\dot{\theta}$ , that is, to reduce the stability of the sintering process. Nevertheless, the process turns out to be stable.

Figure 24 shows the results obtained considering the Laplace pressure evaluated by using the stochastic approach, leading to the expression for the sintering stress (23). Results obtained by using the other methodology (which leads to (27) for  $p_L$ ) are qualitatively very similar.

## 6. Conclusions

This work is focused on modeling the evolution of material properties during both hot isostatic pressing (HIP) and free sintering of axisymmetric samples. The effects of both the Laplace pressure, due to the surface tension at the interfaces between the matrix and pores, and the pressure exerted by the gas within the pores on the evolution of the porosity have been investigated for the first time in the literature for such samples. The stability of the process has also been studied.

The Laplace pressure acts in favor of closing the pores, thereby having a beneficial effect on the HIP process by reducing sintering times. Discrepancies in the estimates of such times and in the residual porosity, evaluated by either neglecting or accounting for the Laplace pressure, are studied. It is highlighted that this action cannot be neglected whenever the sintered material has a high strain rate

sensitivity and a small radius of its particles. Indeed, HIP of nanopowders turns out to be very sensitive to the Laplace pressure. This is particularly important for nanopowdered ceramics and nanoparticles of aluminum-zinc-magnesium-copper alloy, which are widely employed in industrial sintering processes.

The gas pressure acting within the pores strongly affects the sintering process only in its third (and final) phase in which, for porosity less than the closure porosity (which is usually on the order of 10%), the pores are basically isolated. During this phase, as the relative density increases the gas pressure in the closed pores also increases, acting “against” the sintering process. This in turn increases the sintering time and can prevent the HIP process from reaching the desired final porosity in the sample. Obviously, the higher the applied pressure the stronger this effect is. This confirms expectations, namely that the effects of the gas pressure must be accounted for whenever the desired final porosities are relatively small (precise evaluation giving information about the relationship between such gas pressure and the smallness of the desired porosity may be obtained through our model).

The stability of the process has been studied by perturbing the rate of change of the porosity and the Laplace pressure, as well as the gas pressure in the pores. While the effect of the former is to slightly increase the stability of the sintering process, the latter reduces the stability. Nevertheless, the process turns out to be stable.

### Appendix: Free sintering

The case of free sintering corresponds to a condition frequently met in industrial processes. In these cases, there is no applied external pressure, so that the shrinkage is due only to the sintering stress,  $p_L$ .

In the case under examination, the stress and strain-rate tensors are purely hydrostatic. Thus, free sintering can be regarded as a particular case of isostatic pressing, with null external loading stress. The evolution law for the porosity may be obtained from (19), simply by substituting  $\sigma = 0$ :

$$\dot{\theta} = -\left(\frac{p_L - p_I}{\sigma_0 A}\right)^{1/m} \dot{\varepsilon}_0 \psi^{-(1+m)/2m} (1 - \theta)^{(3m-1)/2m}. \quad (\text{A.1})$$

The introduction of the dimensionless specific time  $\tau_L$ , defined by (20), yields the following normalization of (A.1):

$$\frac{\partial \theta}{\partial \tau_L} = (p_L - p_I)^{1/m} \psi^{-(1+m)/2m} (1 - \theta)^{(3m-1)/2m}. \quad (\text{A.2})$$

**A.1 Effect of the Laplace pressure.** Because for free sintering the gas pressure in the pores is neglected, the only force driving the process is the Laplace pressure, the choice of the approach used to derive its expression (stochastic or dissipation averaging; see Section 2.2) has a strong influence on the result. This issue may be studied in the sequel.

*Sintering stress by using a stochastic approach* ( $p_L = (3\alpha/r_0)(1 - \theta)^2$ , see Section 2.3(1)). By substituting (23) into (A.2), it may be written as follows:

$$\frac{\partial \theta}{\partial \tau_L} = \left(\frac{3\alpha}{r_0}\right)^{1/m} \psi^{-(1+m)/2m} (1 - \theta)^{3((m+1)/2m)}. \quad (\text{A.3})$$

In order to compare the evolution of the porosity for this case, for the three different models considered in Section 2.2 (Skorohod, Cocks, Castañeda–Duva–Crow, and McMeeking; the latter two models coincide

for isostatic pressing), Figure 25 shows the evolution of the porosity for different values of the strain rate sensitivity,  $m$ .

It is worth noting that the results obtained for the three considered models are fairly different. This is due to the different expressions for the normalized bulk modulus  $\psi$ . Figure 2 shows that the Cocks model, for  $m = 1$ , gives the highest values of  $\psi$  in the whole range of interesting porosities. For such values of  $\psi$ , (A.3) gives lower values of the rate of change of the porosity  $\dot{\theta}$ , corresponding to higher sintering times. Because the Skorohod model introduces smaller values of  $\psi$ , the sintering times obtained by adopting such a model are the shortest.

In Figure 25, the time evolution of the porosity, evaluated for the different models and for different values of the parameter  $m$ , is plotted. Whenever  $m$  decreases, Figure 2 shows that the values of the normalized bulk modulus  $\psi$  obtained by using the Castañeda model increase, while those coming from the Cocks model decrease. The same figure shows that, for lower values of  $m$ , the Castañeda model gives values of  $\psi$  lower than those obtained by using the Cocks expression for the same item. Hence, employment of the Cocks model gives sintering times lower than those obtained by using the approach of Castañeda. Also from Figure 25, note that when  $m$  tends to zero (ideal plastic behavior), the time-porosity graph has a steep knee.

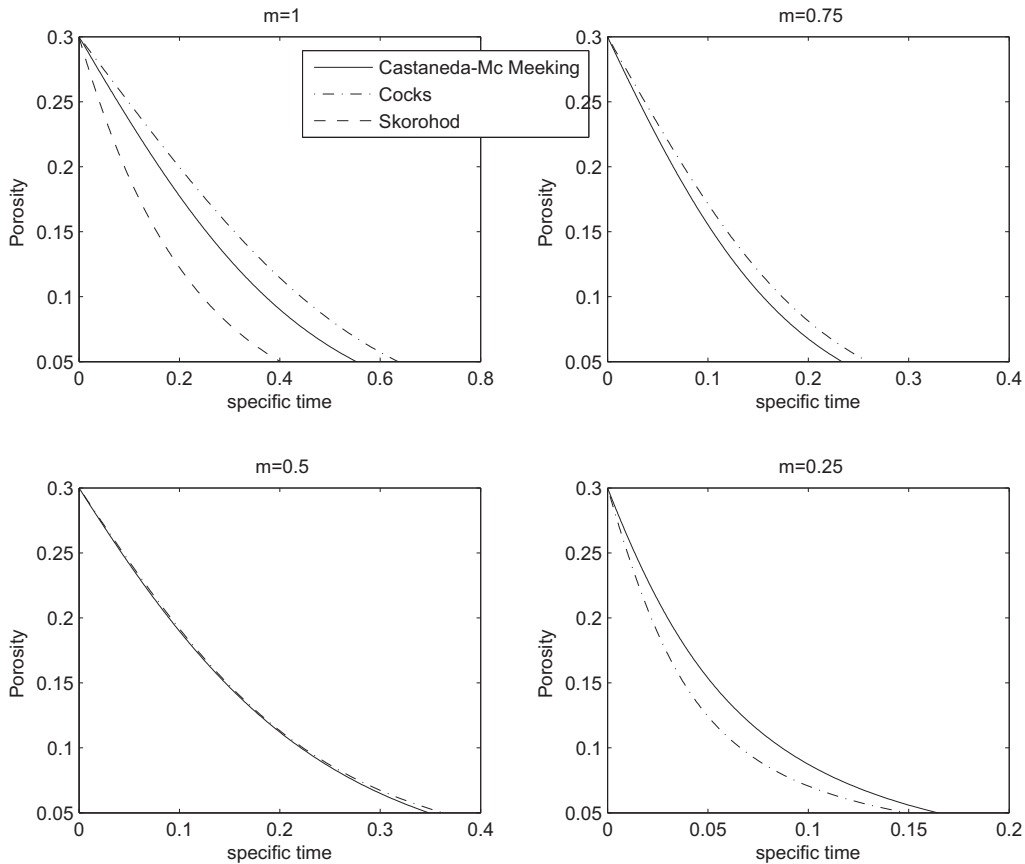


**Figure 25.** Free sintering evolution of porosity for different values of  $m$ , with  $p_L = (3\alpha/r_0)(1 - \theta)^2$ .



Sintering stress from dissipation averaging (that is,  $p_L = (2\alpha/r_0)\sqrt{(3/2)\psi(\theta)\theta/(1-\theta)}$ , see Section 2.3(2)). In this case, expression (A.1), which holds for  $m = 1$  only, reduces to

$$\dot{\theta} = -\frac{\dot{\varepsilon}_0}{\sigma_0 A} \frac{2\alpha}{r_0} \sqrt{\frac{3}{2} \frac{\theta(1-\theta)}{\psi(\theta)}}. \quad (\text{A.4})$$

In the considered range of porosity, the resulting values of the Laplace pressure may be shown to be lower than those obtained by virtue of the expression derived by the stochastic approach (see Figure 5), and hence the sintering times are higher.

**A.2 Effect of the gas pressure in the pores.** In the case of free sintering, the stress due to the external (relative) pressure is  $\sigma = 0$ ; the total driving force of the problem is thus given by the sum of a positive contribution, the Laplace pressure  $p_L$ , and the gas pressure in the pores, which gives a “negative” contribution.

Since the applied external pressure is equal to the standard atmospheric pressure, at the closure porosity  $\theta_C$ ,  $p_I = 0$ . Hence the gas pressure in the pores is usually negligible with respect to the interstitial pressure,  $p_L$ , and the condition (31) is not reached. More precisely, it can be attained for values of grain size not used in real sintering processes.

Figure 26 shows the evolution of the porosity for a free sintering process in two cases:

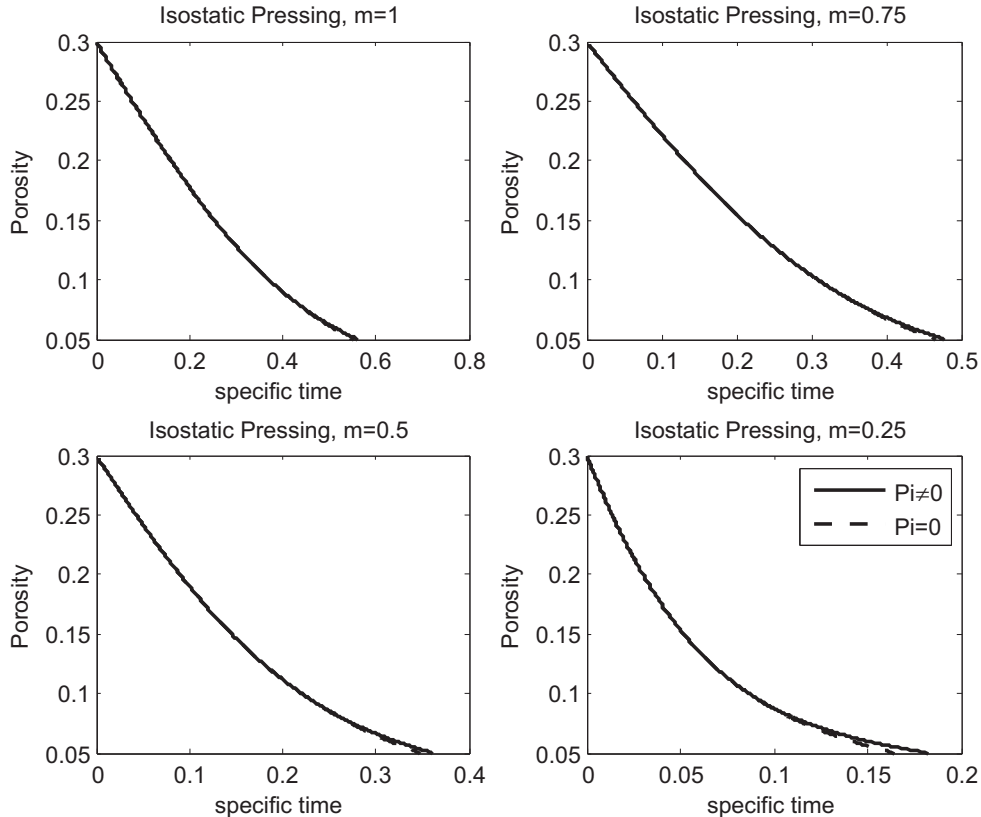


**Figure 26.** Free sintering evolution of porosity for different values of  $m$ .

- accounting for the whole driving force (the dashed line)  $|p_L - p_I|$  and
- neglecting the gas pressure in the pores (the dotted line), that is, the driving force is considered to be only  $p_L$ .

It is evident that the gap between the two curves is negligible.

**A.3 Influence of temperature on free sintering time.** In this paper the sintering processes are assumed to be at constant temperature. In fact, preheated electric ovens are employed in industrial processes, whose thermal capacity may be regarded infinitely large with respect to that of any specimen under consideration. Hence, the temperature remains constant during sintering.

In this section, temperatures are normalized by using the dimensionless specific temperature  $T^*$ , defined as

$$T^* := \frac{T}{T_{\text{melting}}}. \quad (\text{A.5})$$

There are two main phenomena that determine the influence of the temperature on free sintering processes:

- (1) For lower values of  $m$  ( $m \rightarrow 0$ ), the material behavior is almost plastic, and yet it feels the effects of the temperature more than for higher values of the parameter  $m$  (see Figure 27).

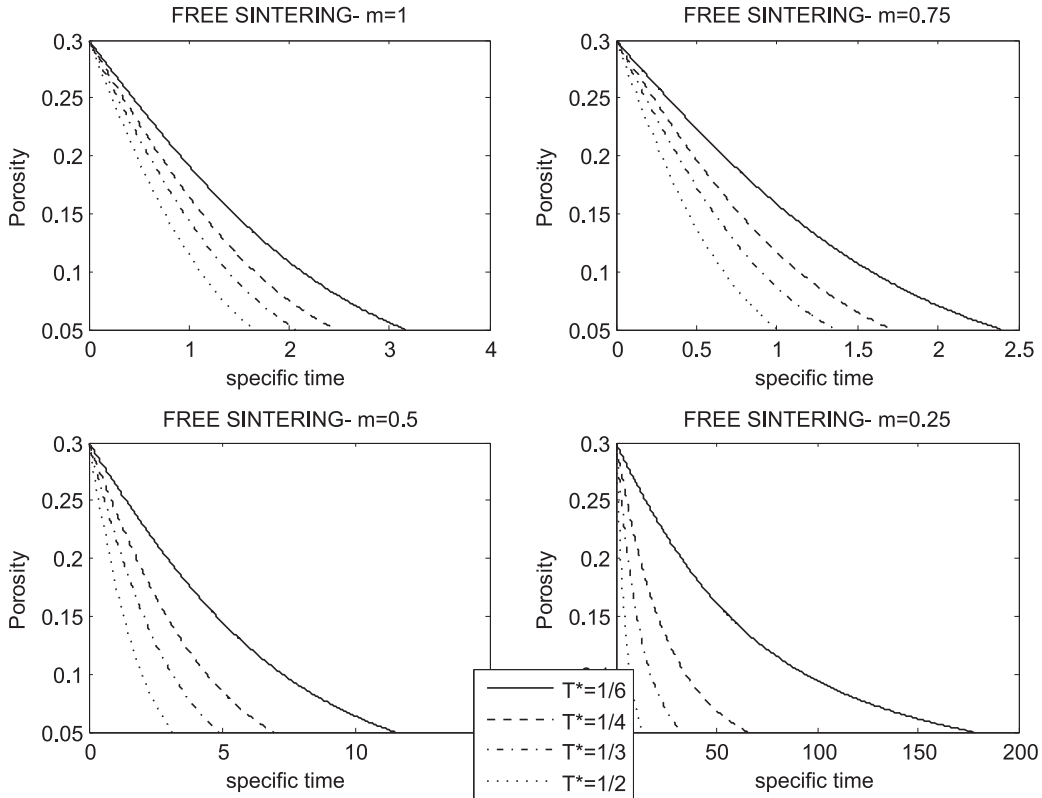


**Figure 27.** Free sintering evolution of porosity for different values of the specific temperature.

- (2) The material behavior is affected by the temperature; thus the value of the parameter  $m$  should be a function of the temperature.

The present model takes into account only the first phenomenon; the implicit dependence on the temperature is given by  $A = \tilde{A}(T)$  [Ashby 1990] and the material constant  $A$ , appearing in (A.1), is raised to  $1/m$ .

Figure 27 shows the evolution of the porosity, evaluated by using the Castañeda model and for the expression of  $p_L$  derived by the stochastic approach, for different values of the strain rate sensitivity,  $m$ , and for different specific temperatures,  $T^*$ . It is evident that, when the temperature increases, the sintering time does decrease. This reduction becomes more important for lower values of the parameter  $m$ .

### Notation

$\sigma_{ij}$	Components of the stress tensor
$\sigma'_{ij}$	Components of the deviatoric stress tensor
$\dot{\epsilon}_{ij}$	Components of the strain rate tensor
$\dot{\epsilon}'_{ij}$	Components of the deviatoric strain rate tensor
$\dot{\epsilon}$	First invariant of the strain rate tensor
$p_L$	Laplace pressure (sintering stress)
$p_I$	Gas pressure in the pores
$w$	Effective equivalent strain rate
$\theta$	Porosity
$\psi$	Normalized bulk modulus
$\varphi$	Normalized shear modulus
$\dot{\gamma}$	Measure of the local rate of change in shape
$p$	First invariant of the stress tensor
$\tau$	Measure of the shear stress
$\sigma_r$	Radial stress
$\sigma_z$	Axial stress
$\dot{\epsilon}_r$	Radial strain rate
$\dot{\epsilon}_z$	Axial strain rate
$n^*$	Loading mode parameter
$n$	Strain rate mode parameter
$\sigma(w)$	Effective equivalent stress
$\sigma_0$	Reference stress
$\dot{\epsilon}_0$	Reference strain rate
$A$	Time-dependent material constant
$m$	Strain rate sensitivity
$\rho$	Relative density
$V_{\text{tot}}$	Total volume of sintered material
$V_{\text{matrix}}$	Matrix volume
$V_{\text{pores}}$	Pore volume
$\tau_L$	Dimensionless specific time
SEP	Specific external pressure
$\alpha$	Surface tension

$r_0$	Characteristic radius of the particles
$p_{L0}$	Reference value of the Laplace pressure
$R_1, R_2$	Internal and external radii, respectively, of the hollow sphere used as a schematic for a pore
$V_r$	Radial velocity
$D$	Dissipation potential
$\theta_c$	Closure porosity
$p_{\text{atm}}$	Atmospheric pressure
$t$	Sintering time evaluated by accounting for the Laplace pressure
$t_0$	Sintering time evaluated by neglecting the Laplace pressure
$p^*$	External pressure for which a given value of the discrepancy between $t$ and $t_0$ is obtained
$\theta_r$	Residual porosity at the end of the sintering process, evaluated by accounting for the Laplace pressure
$\theta_{r0}$	Residual porosity at the end of the sintering process, evaluated by neglecting the Laplace pressure
$E\%$	Error on the evaluation on the residual porosity
$\theta_F$	Desired final porosity at the end of the sintering process
$\theta^*$	Limit value of the porosity
$\lambda$	Perturbation growth rate
$\bullet^{(0)}$	Reference solution for $\bullet$
$\delta\bullet$	Perturbation of $\bullet$

### Acknowledgements

Luca Deseri acknowledges the Department of Mathematical Sciences and the Center for Nonlinear Analysis, Carnegie Mellon University, through NSF Grant No. DMS-0635983, as well as financial support from EU grant PIAP-GA-2011-286110-INTERCER2, “Modeling and optimal design of ceramic structures with defects and imperfect interfaces”.

### References

- [Arzt et al. 1983] E. Arzt, M. F. Ashby, and K. E. Easterling, “Practical applications of hotisostatic pressing diagrams: Four case studies”, *Metall. Trans. A* **14**:1 (1983), 211–221.
- [Ashby 1974] M. F. Ashby, “A first report on sintering diagrams”, *Acta Metall.* **22**:3 (1974), 275–289.
- [Ashby 1990] M. F. Ashby, “Background reading, HIP 6.0”, University of Cambridge, 1990.
- [Bigoni and Piccolroaz 2004] D. Bigoni and A. Piccolroaz, “Yield criteria for quasibrittle and frictional materials”, *Int. J. Solids Struct.* **41**:11-12 (2004), 2855–2878.
- [Cocks 1994] A. C. F. Cocks, “Overview no. 117: The structure of constitutive laws for the sintering of fine grained materials”, *Acta Metall. Mater.* **42**:7 (1994), 2191–2210.
- [Coleman and Beere 1975] S. C. Coleman and W. Beere, “The sintering of open and closed porosity in  $UO_2$ ”, *Philos. Mag.* **31**:6 (1975), 1403–1413.
- [Dal Corso and Deseri 2013] F. Dal Corso and L. Deseri, “Residual stresses in random elastic composites: Nonlocal micro-mechanics-based models and first estimates of the representative volume element size”, *Meccanica* **48**:8 (2013), 1901–1923.
- [Deseri and Owen 2003] L. Deseri and D. R. Owen, “Toward a field theory for elastic bodies undergoing disarrangements”, *J. Elasticity* **70**:1-3 (2003), 197–236.
- [Deseri and Owen 2010] L. Deseri and D. R. Owen, “Submacroscopically stable equilibria of elastic bodies undergoing disarrangements and dissipation”, *Math. Mech. Solids* **15**:6 (2010), 611–638.
- [Deseri and Owen 2013] L. Deseri and D. R. Owen, “Moving interfaces that separate loose and compact phases of elastic aggregates: A mechanism for drastic reduction or increase in macroscopic deformation”, *Continuum Mech. Thermodyn.* **25**:2-4 (2013), 311–341.

- [Deseri et al. 2013] L. Deseri, M. D. Paola, M. Zingales, and P. Pollaci, “Power-law hereditariness of hierarchical fractal bones”, *Int. J. Numer. Meth. Biomed. Eng.* **29**:12 (2013), 1338–1360.
- [Duva and Crow 1992] J. M. Duva and P. D. Crow, “The densification of powders by power-law creep during hot isostatic pressing”, *Acta Metall. Mater.* **40**:1 (1992), 31–35.
- [Gokce and Findik 2008] A. Gokce and F. Findik, “Mechanical and physical properties of sintered aluminum powders”, *JAMME* **30**:2 (2008), 157–164.
- [Green et al. 2008] D. J. Green, O. Guillon, and J. Rödel, “Constrained sintering: A delicate balance of scales”, *J. Eur. Ceram. Soc.* **28**:7 (2008), 1451–1466.
- [Guillon et al. 2008] O. Guillon, S. Cao, J. Chang, L. Wondraczek, and A. R. Boccaccini, “Effect of uniaxial load on the sintering behaviour of 45S5 Bioglass powder compacts”, *J. Eur. Ceram. Soc.* **31**:6 (2008), 999–1007.
- [Hutchinson et al. 1978] J. W. Hutchinson, K. W. Neale, and A. Needleman, “Sheet necking, I: Validity of plane stress assumptions of the long-wavelength approximation”, pp. 111–126 in *Mechanics of Sheet Metal Forming*, edited by D. P. Koistinen and N. M. Wang, Plenum, New York, 1978.
- [Kumikov and Khokonov 1983] V. K. Kumikov and K. B. Khokonov, “On the measurement of surface free energy and surface tension of solid metals”, *J. Appl. Phys.* **54**:3 (1983), 1346–1350.
- [Lee et al. 2012] J.-S. Lee, L. Klinger, and E. Rabkin, “Particle rearrangement during sintering of heterogeneous powder mixtures: A combined experimental and theoretical study”, *Acta Mater.* **60**:1 (2012), 123–130.
- [Maximenko et al. 2012] A. Maximenko, A. Kuzmov, E. Grigoryev, and E. Olevsky, “Direct multi-scale modeling of sintering”, *J. Am. Ceram. Soc.* **95**:8 (2012), 2383–2388.
- [Muhlburger and Paschen 1993] M. Muhlburger and P. Paschen, “Liquid phase sintering of AlZnMgCu alloys”, *Z. Metallk.* **84**:5 (1993), 346–350.
- [Munir et al. 2006] Z. A. Munir, U. Anselmi-Tamburini, and M. Ohyanagi, “The effect of electric field and pressure on the synthesis and consolidation of materials: A review of the spark plasma sintering method”, *J. Mater. Sci.* **41**:3 (2006), 763–777.
- [Olevsky 1998] E. A. Olevsky, “Theory of sintering: From discrete to continuum”, *Mater. Sci. Eng. R.* **23**:2 (1998), 41–100.
- [Olevsky and Molinari 2000] E. A. Olevsky and A. Molinari, “Instability of sintering of porous bodies”, *Int. J. Plast.* **16**:1 (2000), 1–37.
- [Olevsky and Molinari 2006] E. A. Olevsky and A. Molinari, “Kinetics and stability in compressive and tensile loading of porous bodies”, *Mech. Mater.* **38**:4 (2006), 340–366.
- [Olevsky et al. 2006] E. A. Olevsky, V. Tikare, and T. Garino, “Multi-scale study of sintering: A review”, *J. Am. Ceram. Soc.* **89**:6 (2006), 1914–1922.
- [Paola and Zingales 2011] M. D. Paola and M. Zingales, “Fractional differential calculus for the 3D mechanically-based non-local elasticity”, *Int. J. Multiscale Com.* **9**:5 (2011), 579–597.
- [Paola and Zingales 2012] M. D. Paola and M. Zingales, “Exact mechanical models of fractional hereditary materials”, *J. Rheol.* **56**:5 (2012), 983–1004.
- [Paola et al. 2013] M. D. Paola, F. P. Pinnola, and M. Zingales, “A discrete mechanical model of fractional hereditary materials”, *Meccanica* **48**:7 (2013), 1573–1586.
- [Piccolroaz et al. 2006a] A. Piccolroaz, D. Bigoni, and A. Gajo, “An elastoplastic framework for granular materials becoming cohesive through mechanical densification, I: Small strain formulation”, *Eur. J. Mech. A Solids* **25**:2 (2006), 334–357.
- [Piccolroaz et al. 2006b] A. Piccolroaz, D. Bigoni, and A. Gajo, “An elastoplastic framework for granular materials becoming cohesive through mechanical densification, II: The formulation of elastoplastic coupling at large strain”, *Eur. J. Mech. A Solids* **25**:2 (2006), 358–369.
- [Ponte Castañeda 1991] P. Ponte Castañeda, “The effective mechanical properties of nonlinear isotropic composites”, *J. Mech. Phys. Solids* **39**:1 (1991), 45–71.
- [Sankar et al. 2011] U. Sankar, M. Satgunam, M. Amiryani, R. Singh, and W. D. Teng, “Sintering and densification behavior of ZnO-doped Y-TZP ceramics”, *Appl. Mech. Mater.* **83** (2011), 197–203.
- [Schaffer et al. 2001] G. B. Schaffer, S. H. Huo, J. Drennan, and G. J. Auchterionie, “The effect of trace elements on the sintering of an Al-Zn-Mg-Cu ALLOY”, *Acta Mater.* **49**:14 (2001), 2671–2678.

- [Scherer 2001] G. W. Scherer, “Viscous sintering”, pp. 9536–9540 in *Encyclopedia of materials: Science and technology*, 2nd ed., edited by K. H. J. Buschow et al., Elsevier, Oxford, 2001.
- [Schwarz et al. 2012] S. Schwarz, A. M. Thron, J. Rufner, K. van Benthem, and O. Guillon, “Low temperature sintering of nanocrystalline zinc oxide: Effect of heating rate achieved by field assisted sintering/spark plasma sintering”, *J. Am. Ceram. Soc.* **95**:8 (2012), 2451–2457.
- [Skorohod 1972] V. V. Skorohod, *Rheological basis of the theory of sintering*, Naukova Dumka, Kiev, 1972.
- [Sofronis and McMeeking 1992] P. Sofronis and R. M. McMeeking, “Creep of power-law material containing spherical voids”, *J. Appl. Mech.* **59**:2S (1992), 88–95.
- [Swinkels and Ashby 1981] F. B. Swinkels and M. F. Ashby, “A second report on sintering diagrams”, *Acta Metall.* **29**:2 (1981), 259–281.
- [Swinkels et al. 1983] F. B. Swinkels, D. S. Wilkinson, E. Arzt, and M. F. Ashby, “Mechanisms of hot-isostatic pressing”, *Acta Metall.* **31**:11 (1983), 1829–1840.
- [Wakai 2013] F. Wakai, “Mechanics of viscous sintering on the micro- and macro-scale”, *Acta Mater.* **61**:1 (2013), 239–247.
- [Wakai et al. 2007] F. Wakai, K. Chihara, and M. Yoshida, “Anisotropic shrinkage induced by particle rearrangement in sintering”, *Acta Mater.* **55**:13 (2007), 4553–4566.
- [Wilkinson 1988] D. S. Wilkinson, “A pressure-sintering model for the densification of polar firn and glacier ice”, *J. Glaciol.* **34**:116 (1988), 40–45.
- [Wolff et al. 2012] C. Wolff, S. Mercier, H. Couque, and A. Molinari, “Modeling of conventional hot compaction and spark plasma sintering based on modified micromechanical models of porous materials”, *Mech. Mater.* **49** (2012), 72–91.

Received 8 Jul 2013. Revised 9 Sep 2013. Accepted 6 Oct 2013.

LAURA GALUPPI: [laura.galuppi@unipr.it](mailto:laura.galuppi@unipr.it)

*Dipartimento di Ingegneria Industriale, Università degli Studi di Parma, Viale G. P. Usberti 181/A, 43124 Parma, Italy*

LUCA DESERI: [deseri@andrew.cmu.edu](mailto:deseri@andrew.cmu.edu)

*DICAM, Group of Solid and Structural Mechanics, University of Trento, via Mesiano 77, 38123 Trento, Italy*

and

*Department of Civil and Environmental Engineering and Department of Mechanical Engineering, Carnegie Mellon University, 5000 Forbes Avenue, Pittsburgh, PA 15213, United States*

and

*Department of Nanomedicine, TMHRI-, The Methodist Hospital Research Institute, 6565 Fannin Street, MS B-490, Houston, TX 77030, United States*

# JOURNAL OF MECHANICS OF MATERIALS AND STRUCTURES

[msp.org/jomms](http://msp.org/jomms)

Founded by Charles R. Steele and Marie-Louise Steele

## EDITORIAL BOARD

ADAIR R. AGUIAR University of São Paulo at São Carlos, Brazil  
KATIA BERTOLDI Harvard University, USA  
DAVIDE BIGONI University of Trento, Italy  
IWONA JASIUK University of Illinois at Urbana-Champaign, USA  
THOMAS J. PENCE Michigan State University, USA  
YASUhide SHINDO Tohoku University, Japan  
DAVID STEIGMANN University of California at Berkeley

## ADVISORY BOARD

J. P. CARTER University of Sydney, Australia  
R. M. CHRISTENSEN Stanford University, USA  
G. M. L. GLADWELL University of Waterloo, Canada  
D. H. HODGES Georgia Institute of Technology, USA  
J. HUTCHINSON Harvard University, USA  
C. HWU National Cheng Kung University, Taiwan  
B. L. KARIHALOO University of Wales, UK  
Y. Y. KIM Seoul National University, Republic of Korea  
Z. MROZ Academy of Science, Poland  
D. PAMPLONA Universidade Católica do Rio de Janeiro, Brazil  
M. B. RUBIN Technion, Haifa, Israel  
A. N. SHUPIKOV Ukrainian Academy of Sciences, Ukraine  
T. TARNAI University Budapest, Hungary  
F. Y. M. WAN University of California, Irvine, USA  
P. WRIGGERS Universität Hannover, Germany  
W. YANG Tsinghua University, China  
F. ZIEGLER Technische Universität Wien, Austria

**PRODUCTION** [production@msp.org](mailto:production@msp.org)

SILVIO LEVY Scientific Editor

Cover photo: Ev Shafir

---

See [msp.org/jomms](http://msp.org/jomms) for submission guidelines.

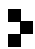
---

JoMMS (ISSN 1559-3959) at Mathematical Sciences Publishers, 798 Evans Hall #6840, c/o University of California, Berkeley, CA 94720-3840, is published in 10 issues a year. The subscription price for 2014 is US\$555/year for the electronic version, and \$710/year (+\$60, if shipping outside the US) for print and electronic. Subscriptions, requests for back issues, and changes of address should be sent to MSP.

---

JoMMS peer-review and production is managed by EditFLOW® from Mathematical Sciences Publishers.

PUBLISHED BY

 **mathematical sciences publishers**  
nonprofit scientific publishing

<http://msp.org/>

© 2014 Mathematical Sciences Publishers

# Journal of Mechanics of Materials and Structures

Volume 9, No. 1

January 2014

---

- Improved thermoelastic coefficients of a novel short fuzzy fiber-reinforced composite with wavy carbon nanotubes**  
SHAILESH I. KUNDALWAL and MANAS C. RAY 1
- Moment Lyapunov exponents and stochastic stability of coupled viscoelastic systems driven by white noise**  
JIAN DENG, WEI-CHAU XIE and MAHESH D. PANDEY 27
- Combined effects of interstitial and Laplace pressure in hot isostatic pressing of cylindrical specimens**  
LAURA GALUPPI and LUCA DESERI 51
- Planar grained structures with traction-smoothing inclusions: an elastostatic numerical analysis for shear and torsion**  
SHMUEL VIGDERGAUZ 87
- Continuous contact problem for two elastic layers resting on an elastic half-infinite plane**  
ERDAL ÖNER and AHMET BIRINCI 105



1559-3959(2014)9:1;1-9